

**SIMULTANEOUS ADSORPTION AND DEGRADATION OF ANILINE
USING MAGNETIC MULTIWALLED CARBON NANOTUBES**

LIM JIA XIN

**A project report submitted in partial fulfilment of the
requirements for the award of Bachelor of Engineering
(Honours) Chemical Engineering**

**Lee Kong Chian Faculty of Engineering and Science
Universiti Tunku Abdul Rahman**

April 2020

DECLARATION

I hereby declare that this project report is based on my original work except for citations and quotations which have been duly acknowledged. I also declare that it has not been previously and concurrently submitted for any other degree or award at UTAR or other institutions.

Signature : Li

Name : Lim Jia Xin

ID No. : 15UEB03723

Date : 18 May 2020

APPROVAL FOR SUBMISSION

I certify that this project report entitled “**SIMULTANEOUS ADSORPTION AND DEGRADATION OF ANILINE USING MAGNETIC MULTIWALLED CARBON NANOTUBES**” was prepared by **LIM JIA XIN** has met the required standard for submission in partial fulfilment of the requirements for the award of Bachelor of Engineering (Honours) Chemical Engineering at Universiti Tunku Abdul Rahman.

Approved by,

Signature : 

Supervisor : Ts. Dr. Shuit Siew Hoong

Date : 18 May 2020

Signature : 

Co-Supervisor : ChM. Ts. Dr. Tee Shiau Foon

Date : 18 May 2020

The copyright of this report belongs to the author under the terms of the copyright Act 1987 as qualified by Intellectual Property Policy of Universiti Tunku Abdul Rahman. Due acknowledgement shall always be made of the use of any material contained in, or derived from, this report.

© 2020, Lim Jia Xin. All right reserved.

ACKNOWLEDGEMENTS

I would like to thank everyone who had contributed to the successful completion of this project. I would like to express my gratitude to my research supervisor, Ts. Dr. Shuit Siew Hoong and co-supervisor, ChM. Ts. Dr. Tee Shiau Foon for their invaluable advice, guidance and enormous patience throughout the development of research.

In addition, I would also like to express my gratitude to my loving parents and friends who had helped and given me encouragement throughout the period in completing my final year project.

Lastly, I offer my best regards to all who had supported me towards the completion of the final year project.

ABSTRACT

Aniline which is widely used as raw material in different industries is one of the main industrial pollutants leading to the deterioration of water quality. Thus, removal of aniline by simultaneous adsorption and degradation using magnetic multiwalled carbon nanotubes, MWCNTs-Fe₃O₄ was investigated in this study. MWCNTs-Fe₃O₄ were synthesised using direct doping method and characterized using X-ray diffraction (XRD), Fourier-transform infrared spectroscopy (FTIR), scanning electron microscopy coupled with energy dispersive X-ray (SEM-EDX), Brunauer–Emmett–Teller (BET) and thermogravimetric analysis (TGA). The effects of several process parameters such as solution pH (pH 2-10), MWCNTs-Fe₃O₄ dosage (5-20 mg) and H₂O₂ dosage (4-16 mM) were studied. Solution pH of pH 6 was found to be the best for aniline adsorption while aniline degradation efficiency decreased with increasing pH. Both adsorption and degradation efficiency increased with increasing MWCNTs-Fe₃O₄ dosage. Adsorption was not affected by H₂O₂ dosage because H₂O₂ dosage was found to be an insignificant factor for aniline adsorption. For degradation of aniline, low H₂O₂ dosage (6.43 mM) was sufficient. Response surface methodology (RSM) was applied to optimize the aniline adsorption and degradation efficiency. The optimum condition was found at solution pH of 3.71, MWCNTs-Fe₃O₄ dosage of 14.47 mg and H₂O₂ dosage of 6.43 mM. The actual adsorption and degradation efficiency obtained at this condition was 59.61 % and 21.21 % respectively. It could be concluded that simultaneous adsorption and degradation using MWCNTs-Fe₃O₄ could be one of the feasible methods to remove aniline from wastewater.

2.2.2	Single-walled Carbon Nanotubes (SWCNTs)	17
2.2.3	Multiwalled Carbon Nanotubes (MWCNTs)	19
2.2.4	Comparison of Single-walled Carbon Nanotubes and Multiwalled Carbon Nanotubes	22
2.3	Synthesis of Magnetic Multiwalled Carbon Nanotubes (MWCNTs-Fe ₃ O ₄) by Direct Doping Method	22
2.4	Characterization Study	23
2.4.1	Fourier Transform Infrared Spectroscopy (FTIR)	23
2.4.2	X-Ray Diffraction (XRD)	24
2.4.3	Scanning Electron Microscope Coupled with Energy Dispersive X-Ray (SEM-EDX)	25
2.4.4	Brunauer–Emmett–Teller (BET)	26
2.4.5	Thermogravimetric Analysis (TGA)	26
2.4.6	UV-visible (UV-vis) Spectroscopy	27
2.5	Parameter Study	28
2.5.1	Effects of Solution pH	28
2.5.2	Effects of Temperature	30
2.5.3	Effects of Initial Concentration of Aniline	31
2.5.4	Effects of MWCNTs-Fe ₃ O ₄ dosage	32
2.5.5	Effects of H ₂ O ₂ Dosage	33
3	METHODOLOGY AND WORK PLAN	34
3.1	Materials and Chemicals	34
3.2	Equipment	35
3.3	Overall Experiment Flowchart	35
3.4	Preparation of MWCNTs-Fe ₃ O ₄	36

3.4.1	Pre-treatment and functionalization of MWCNTs	37
3.4.2	Direct Doping	37
3.5	Characterization of pristine MWCNTs, MWCNTs-COOH and MWCNTs-Fe ₃ O ₄	37
3.5.1	FTIR	38
3.5.2	XRD	38
3.5.3	SEM-EDX	38
3.5.4	BET	38
3.5.5	TGA	39
3.6	Simultaneous Adsorption and Degradation of Aniline using MWCNTs-Fe ₃ O ₄	39
3.7	Statistical Analysis and Optimization Using Design of Experiments (DOE)	40
4	RESULTS AND DISCUSSION	42
4.1	Characterization of MWCNTs, MWCNTs-COOH and MWCNTs-Fe ₃ O ₄	42
4.1.1	FTIR Results	42
4.1.2	XRD Results	43
4.1.3	SEM-EDX results	44
4.1.4	BET Results	46
4.1.5	TGA Results	47
4.2	Statistical Analysis and Optimization Study	49
4.2.1	Regression Analysis	49
4.3	Response Surface (RSM) analysis	55
4.3.1	Effect of solution pH on Adsorption Efficiency of Aniline	55
4.3.2	Effect of Solution pH on Degradation Efficiency of Aniline	57
4.3.3	Effect of MWCNTs-Fe ₃ O ₄ dosage on Adsorption Efficiency of Aniline	58
4.3.4	Effect of MWCNTs-Fe ₃ O ₄ dosage on Degradation Efficiency of Aniline	59

4.3.5	Effect of H ₂ O ₂ dosage on Degradation Efficiency of Aniline	60
4.3.6	Optimization of Process Parameter	62
4.4	Effects of Simultaneous Adsorption and Degradation of Aniline on the Structure of MWCNTs-Fe ₃ O ₄	64
5	CONCLUSIONS AND RECOMMENDATIONS	65
5.1	Conclusions	65
5.2	Recommendations for Future Work	66
	REFERENCES	67
	APPENDICES	74

LIST OF TABLES

Table 2.1:	Reaction Mechanism of Fenton Process and Corresponding Rate Constants at pH 4 (Shen et al., 2017)	12
Table 2.2:	Summary of Different Wastewater Treatment Method (Ramachandran et al., 2013)	14
Table 2.3:	Classification of SWCNTs (Nanot et al., 2013)	18
Table 2.4:	Comparison of Single-walled Carbon Nanotubes and Multiwalled Carbon Nanotubes (Sarangdevot and Sonigara, 2015)	22
Table 3.1:	List of Chemicals and Their Specifications	34
Table 3.2:	List of Instruments and Functions	35
Table 3.3:	Coded and Actual Values of Process Parameters in the Design	41
Table 3.4:	Design Matrix of Experiments with CCD Coded Factors	41
Table 4.1:	Atomic Percent for MWCNTs, MWCNTs-COOH and MMWCNTs	46
Table 4.2:	BET Results for Samples	46
Table 4.3:	Experiment Design Conditions and Their Respective Adsorption and Degradation Efficiency	50
Table 4.4:	ANOVA result for Response Surface Model for Adsorption Efficiency of Aniline	51
Table 4.5:	ANOVA result for Response Surface Model for Degradation Efficiency of Aniline	53
Table 4.6:	Constraints for Optimization of Aniline Adsorption and Degradation Efficiencies	62
Table 4.7:	Model Validation Conducted at Optimum Condition Generated by Design Expert	63

Table A.1:	Volume of Aniline Stock Solution Required to Prepare Various Concentration of Aniline in 15 ml solution	75
Table D.1:	Volume of H ₂ O ₂ Required to Prepare Different Dosage in 15 ml solution	79

LIST OF FIGURES

Figure 1.1:	U.S. Synthetic & Bio-Based Aniline Market Size, By Application, 2012 – 2024 (USD Million) (Global Market Insights, 2018)	2
Figure 2.1:	Zone of Operation in a Facultative Pond (Department of Natural Resources & Environment - State of Michigan, 2010)	9
Figure 2.2:	Basic Terms of Adsorption (Worch, 2012)	10
Figure 2.3:	Reaction Mechanism for the Fenton process (Zhang et al., 2019)	13
Figure 2.4:	Mechanism for Heterogeneous Fenton Process (Zhang et al., 2019)	14
Figure 2.5:	3D Structure of the Buckminster Fullerene Molecule (Sarangdevot and Sonigara, 2015)	16
Figure 2.6:	Structure of Carbon Nanotube (Sarangdevot and Sonigara, 2015)	16
Figure 2.7:	Formation of SWCNT from a graphene sheet (Wang, Huang and Lieber, 2002)	17
Figure 2.8:	Structure of MWCNTs (Rafique et al., 2015)	19
Figure 2.9:	Schematic Draft of the Layer Arrangement of (A) Parchment Model and (B) Russian Model (Jurková, 2013)	20
Figure 2.10:	Schematic Grafting of CNTs and Decoration by Fe ₃ O ₄ Nanoparticles (Stoffelbach et al., 2005)	23
Figure 3.1:	Overall Flowchart of Experiment	36
Figure 4.1:	FTIR Spectra of (a) MWCNTs-COOH, (b) MWCNTs-Fe ₃ O ₄	43
Figure 4.2:	XRD Patterns for (a) Pristine MWCNTs, (b) MWCNTs-COOH, (c) Synthesized MWCNTs-Fe ₃ O ₄	44
Figure 4.3:	SEM Images of (a) Pristine MWCNTs, (b) MWCNTs-COOH, (c) MWCNTs-Fe ₃ O ₄	45

Figure 4.4:	TGA Curves for MWCNTs-COOH and MWCNTs-Fe ₃ O ₄	48
Figure 4.5:	Derivative Weight Loss Curve of MWCNTs-COOH	48
Figure 4.6:	Derivative Weight Loss Curve of MWCNTs-Fe ₃ O ₄	49
Figure 4.7:	Actual and Predicted Values of Adsorption Efficiency of Aniline ($R^2=0.9005$)	52
Figure 4.8:	Actual and Predicted Values of Degradation Efficiency of Aniline ($R^2=0.9290$)	55
Figure 4.9:	Effect of solution pH on Adsorption Efficiency of Aniline by MWCNTs-Fe ₃ O ₄ (MWCNTs-Fe ₃ O ₄ dosage= 12.5 mg, H ₂ O ₂ dosage=10 mM)	56
Figure 4.10:	Effect of Solution pH on Degradation Efficiency of Aniline by MWCNTs-Fe ₃ O ₄ (MWCNTs-Fe ₃ O ₄ dosage= 12.5 mg, H ₂ O ₂ dosage=10 mM)	58
Figure 4.11:	Effects of MWCNTs-Fe ₃ O ₄ dosage on Adsorption Efficiency of Aniline by MWCNTs-Fe ₃ O ₄ (Solution pH: pH 6, H ₂ O ₂ dosage=10 mM)	59
Figure 4.12:	Effects of MWCNTs-Fe ₃ O ₄ dosage on Degradation Efficiency of Aniline by MWCNTs-Fe ₃ O ₄ (Solution pH: pH 3.62, H ₂ O ₂ dosage=10 mM)	60
Figure 4.13:	Effects of H ₂ O ₂ dosage on Degradation Efficiency of Aniline by MWCNTs-Fe ₃ O ₄ (Solution pH: pH 3.62, MWCNTs-Fe ₃ O ₄ dosage=8.04 mg)	61
Figure 4.14:	XRD Patterns for (a) Synthesized MWCNTs-Fe ₃ O ₄ (b) Used MWCNTs- Fe ₃ O ₄	64
Figure E.1:	Calibration Curve of Aniline in Distilled Water	80
Figure E.2:	Calibration Curve of Aniline in Ethanol	80

LIST OF SYMBOLS / ABBREVIATIONS

A	absorbance
c	concentration of solution, mol dm ⁻³
$C_{A,24}$	Aniline concentration after 24 hours, mg/L
$C_{A,adsorb}$	Aniline concentration being removed by adsorption, mg/L
$C_{A,degrade}$	Aniline concentration being removed by degradation, mg/L
$C_{A,ethanol}$	Aniline concentration being dissolved in ethanol, mg/L
C_{AO}	Initial concentration of aniline, mg/L
C_{AT}	Total aniline concentration being removed, mg/L
d	interplanar spacing producing the diffraction
K	constant, 0.9
L	average crystalline size, Å
l	dimension of the cell cuvette, cm
P/P_0	relative pressure
X	number of gas molecules adsorbed
X_m	number of gas molecules adsorbed as monolayer
β	peak width at half maximum height resulting from small crystallite size, radians
θ	Angle between beams and the normal to the reflecting plane, °
λ	X-ray wavelength, nm
ε	constant for a particular substance at particular wavelength, dm ³ mol ⁻¹ cm ⁻¹
$\cdot\text{OH}$	hydroxyl radical
1-D	1 dimensional
AOP	advanced oxidation process
BET	Brunauer–Emmett–Teller
CCD	central composite design
CNF	carbon nanofiber

CNTs	carbon nanotubes
Co	Cobalt
CO ₂	carbon dioxide
-COO ⁻	carboxylate anions
-COOH	carboxyl group
Cu	Copper
C _x	carbon cluster corresponding to x carbon atoms
DOE	design of experiment
Fe	iron
Fe ²⁺	iron ions with two positive charges
Fe ³⁺	iron ions with three positive charges
Fe ₃ O ₄	magnetite
FTIR	fourier transform infrared spectroscopy
H ⁺	hydrogen ions
H ₂ O ₂	hydrogen peroxide
HCl	hydrochloric acid
HNO ₃	nitric acid
IR	infrared
MB	methylene blue
MDI	methylene diphenyl diisocyanate
MMWCNTs	magnetic multiwalled carbon nanotubes
MWCNTs	multiwalled carbon nanotubes
MWCNTs-COOH	functionalized multiwalled carbon nanotubes with carboxyl group
MWCNTs-Fe ₃ O ₄	magnetite doped multiwalled carbon nanotubes
NaOH	sodium hydroxide
Ni	Nickel
O ₂	oxygen
OH ⁻	hydroxide ions
pH _{pzc}	point of zero charge pH
pKa	negative base-10 logarithm of acid dissociation constant
RBM	radical breathing mode
RSM	response surface methodology

SEM-EDX	scanning electron microscopy coupled with energy dispersive x-ray
SWCNTs	single-walled carbon nanotubes
TBBPA	tetrabromobisphenol A
TGA	thermogravimetric analysis
UV-vis	UV-visible
XRD	X-ray diffraction

LIST OF APPENDICES

APPENDIX A: Preparation of Various Concentration of Aniline	74
APPENDIX B: Preparation of 0.1 M HCl from a 37 % HCl Solution	76
APPENDIX C: Preparation of 0.1 M NaOH from 97 % NaOH	77
APPENDIX D: Preparation of 0.1 M H ₂ O ₂ from 30 % H ₂ O ₂	78
APPENDIX E: Calibration Curve of Aniline	80

CHAPTER 1

INTRODUCTION

1.1 General Introduction

From waste in daily life to the industrial chemicals, large amounts of pollutants have been discharged into the rivers, lakes, and oceans without proper treatment, causing water pollution become a serious environmental issue. Although about 70% of earth is covered by water, only 2.5% of it is freshwater and only 1% of the freshwater can be accessed easily (Nunez, 2010). There are many sources of water pollution such as the agricultural waste, city sewage and industrial waste. Industry has become the major source of water pollution due to its rapid development. Industry wastes include heavy metals, spent solvents, reactive waste, strong acids and bases, hydrocarbons and organic constituents (SDWF, 2017). Aniline, an organic compound which is widely used as raw materials in different industries is one of the main industrial pollutants causing the deterioration of water quality.

Aniline is a primary aromatic amine which exists as a colourless liquid. It is oily, toxic and poses an unpleasant rotten fish smell. The primary use of aniline is to produce methylene diphenyl diisocyanate (MDI) which is widely uses in different application such as construction, furniture production and transportation. Besides, aniline is also used as raw materials in industry such as rubber processing, agrochemicals, dyestuff and pharmaceutical products (Global Market Insights, 2018). Figure 1.1 indicated a steady increase in the demand of aniline of aniline until year 2024.

The presence of aniline in water resources even in small amount is hazardous to the health of human and aquatic organisms. The probable oral lethal dose in human is 50-500 mg per kg weight of body. Adverse health effect can be caused by exposure to high level of aniline. The major health effect due to high aniline exposure is the formation of methaemoglobin which can further lead to cyanosis (discoloration of skin because of the insufficient oxygenation of blood) (EPA, 2016). Exposing to aniline for long period can lead to health

problems such as liver, kidney and neurological marrow disorders, anorexia and reduction in weight (Kakavandi et al., 2013).

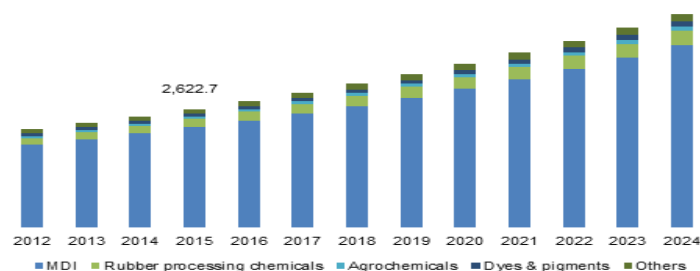


Figure 1.1: U.S. Synthetic & Bio-Based Aniline Market Size, By Application, 2012 – 2024 (USD Million) (Global Market Insights, 2018)

Different methods which are commonly used to remove aniline from wastewater including photo-catalysis, biodegradation, advanced oxidation, electrolysis, ligand exchanger and adsorption. Among the methods, adsorption is one of the effective method to separate a large variety of organic pollutant from the wastewater. Adsorbent such as ion exchange resins, zeolites, polymeric adsorbent or multiwalled carbon nanotubes (MWCNTs) are used in adsorption process (Kakavandi et al., 2013). Apart from the adsorption method, advanced oxidation process (AOPs) is proven as an effective method to degrade aniline. Fenton process (one of the AOPs) is a catalytic process which ferrous ion (Fe^{2+}) reacts with hydrogen peroxide (H_2O_2) (Huang et al., 2012). During Fenton Process, iron species catalyse the decomposition of H_2O_2 to generate free hydroxyl free radical ($\cdot\text{OH}$) which possesses high oxidizing ability to degrade the aniline in water (Liu et al., 2016). Even though both the adsorption method and Fenton process are effective to remove aniline from wastewater, both of them has their disadvantages respectively. Hence, simultaneous adsorption and degradation of aniline using magnetic multiwalled carbon nanotubes is studied to improve the existing method.

1.2 Importance of the Study

This study is important to identify the effectiveness of simultaneous adsorption and degradation of aniline in wastewater. The method of adsorption and AOPs has been studied extensively by researchers. Only few studies reported on the

simultaneous adsorption and degradation method. Hence, this research can be used to determine the range of operating condition which can be further used as reference in future research to improve this simultaneous removal method.

1.3 Problem Statement

One of the common methods used for wastewater treatment is adsorption. The adsorbent which are commonly used in wastewater treatment include activated clay and other waste materials such as coal fly ash, coal bottom ash and sawdust from industries and agricultural products (Moradi, 2013). However, these adsorbents have some limitation such as low surface area for the adsorption, low selectivity and the adsorption kinetics. Activated carbon has better performance compared to these adsorbents due to its large specific surface area (500 to 1500 m²/g) and electric charge to adsorb different polar compound (Jackson, 2014). However, activated carbon is expensive and have some disadvantages. For examples, there are a lot of small pores (microspores) in activated carbon which cannot be accessed by bulky organic molecules. In addition, its affinity of adsorption for polar organic compounds which has low molecular weight.

Therefore, a possible solution to this issue is to use multiwalled carbon nanotubes (MWCNTs) as adsorbent. Compared to activated carbon, carbon nanotubes have the structures which are more uniform, hence the adsorption sites of carbon nanotubes are well defined and more available to the pollutant such as aniline. Even though the specific surface area of activated carbon and carbon nanotubes are comparable, the adsorption capacities for carbon nanotubes are higher since the carbon nanotubes have larger pores in bundles and higher amount of sorption sites. Furthermore, carbon nanotubes have wider variety of contaminant-carbon nanotubes interaction such as hydrophobic effect, π - π interactions, hydrogen and covalent bonding, allowing it to adsorb different kinds of polar organic compounds (Zare et al., 2015).

Conventional adsorption process requires additional separation processes to recover the adsorbents from treated wastewater before discharging the water. Apart from that, the adsorbent such as MWCNTs possess smaller size in order to increase the surface area to obtain higher adsorption capacity. Therefore, the trade-off of having the high adsorption capacity is the difficulty

in separating the adsorbent from the water. The separation of the carbon nanotubes from wastewater can be achieved by centrifuge or filtration. However, the additional separation process requires higher operating costs (Abdel Salam et al., 2012).

Magnetic separation technology can be used together with the adsorption process to overcome the difficulty of separation facing by conventional adsorption method. Magnetic multiwalled carbon nanotubes (MMWCNTs) composed of the magnetic particles such as Fe_3O_4 are dispersed on the carbon nanotubes. Introducing magnetic properties to MWCNTs leads to better adsorption performance due to the high adsorption capacity of MWCNTs and separation convenience of magnetic particles. No flocculants are formed and the adsorbent can be separated out within short period (Sivashankar et al., 2014). Besides, MWCNTs act as a support to disperse the Fe_3O_4 .

However, the magnetic adsorption process will still cause the production of secondary waste. Spent carbon adsorbent is a hazardous waste to be disposed and might cause environmental issues since adsorption method is not a destructive method. Treating aniline by using adsorption does not eliminate the aniline pollutant, but only transfers the aniline from the wastewater to the adsorbent phase. One of the promising method to reduce the secondary waste formed is to use the method of simultaneous adsorption coupling with heterogeneous Fenton oxidation. Introduction of Fenton oxidation which is considered as a destructive method in which aniline is degraded into less hazardous material such as CO_2 and H_2O .

Conventional adsorption which involves the thermal regeneration of adsorbents affects the re-adsorptive capacity of the adsorbent. After the adsorbent such as the carbon nanotubes is used for certain period, it is contaminated and the adsorptive capacity of the adsorbent decreases. Hence, the thermal regeneration of the adsorbent is required so that to ensure the re-adsorptive capacity can be achieved. However, the thermal regeneration method can cause the pore structure, functionality and specific surface area of carbon to deteriorate (Kim et al., 2015).

To overcome this problem, simultaneous adsorption coupling with heterogeneous Fenton oxidation can be applied. Thermal regeneration of the

carbon adsorbent can be replaced by in situ regeneration using heterogeneous Fenton oxidation-driven regeneration. By introducing this Fenton oxidation-driven regeneration, the OH radicals generated when H_2O_2 reacted with iron on the adsorbent can oxidize and degrade the aniline contaminants at the surface of the adsorbent. In this case, heterogeneous Fenton oxidation is more preferable than homogenous Fenton oxidation due to the wider pH working range and less generation of iron sludge (Kim et al., 2015).

1.4 Aim and Objectives

The ultimate aim of this study is to remove aniline from wastewater to an acceptable level by simultaneous adsorption and degradation of aniline using magnetic multiwalled carbon nanotubes. To achieve the ultimate aim, the objectives of this research study include:

- a. To synthesis magnetic multiwalled carbon nanotubes, MWCNTs- Fe_3O_4 via solvent free direct doping method.
- b. To characterize the synthesized magnetic multiwalled carbon nanotubes, MWCNTs- Fe_3O_4 .
- c. To optimise the process parameters for simultaneous adsorption and degradation of aniline using response surface methodology.

1.5 Scope and Limitation of the Study

The scope of this study includes the synthesis of magnetic multiwalled carbon nanotubes, MWCNTs- Fe_3O_4 through the direct doping method. The characterization of synthesized MWCNTs- Fe_3O_4 was done by X-ray diffraction (XRD), fourier transform infrared spectroscopy (FTIR), scanning electron microscopy coupled with energy dispersive X-ray (SEM-EDX), Brunauer–Emmett–Teller (BET) and thermogravimetric analysis (TGA).

A series of experiment was carried out based on the runs generated by Design Expert software to study the effects of different parameters on simultaneous adsorption and degradation of aniline using magnetic multiwalled carbon nanotubes and to optimize the adsorption and degradation efficiencies using response surface method (RSM) coupled with central composite design (CCD). The parameters include pH, MWCNTs- Fe_3O_4 dosage and H_2O_2 dosage.

The liquid sample analysis will be carried out by analysing the concentration of aniline using UV-vis spectrophotometer.

In fact, besides of pH, MWCNTs-Fe₃O₄ dosage and H₂O₂ dosage, other factors such as initial aniline concentration and temperature also affects the adsorption and degradation efficiency of aniline. However, these factors are not investigated in this study. In this study, UV-visible spectroscopy was used for the liquid sample analysis. However, intermediates of aniline degradation that had benzene ring may contribute to the absorbance at 280 nm and become disturbance while measuring the concentration of aniline.

1.6 Contribution of the Study

Throughout this study, the condition for MWCNTs-Fe₃O₄ synthesis can be used as reference for future research. Besides, the range of process parameters studied and findings obtained in this study can also be used as reference in the future to enhance the adsorption and desorption efficiency of aniline in future research.

1.7 Outline of Report

There are five main chapters in this report. Chapter 1 introduce briefly about aniline and its effect to human and environment as well as some methods to remove aniline. Problem statements, aims and objectives of the study are also included in Chapter 1. The literature reviews, covering the basic principal and knowledge related to this study can be obtained from Chapter 2. In Chapter 3, the required chemicals, equipment and detailed methodology are presented. The results obtained from the experiments and discussions on the results are covered in Chapter 4 while Chapter 5 summarises the study and provides some recommendations.

CHAPTER 2

LITERATURE REVIEW

2.1 Wastewater Treatment Technologies

To reduce the environmental issues caused by the industrial activities, wide variety of technologies including chemical, physical and biological methods are established to treat the wastewater. Common technologies used for wastewater treatment consists of coagulation and flocculation, biodegradation, adsorption and Fenton process.

2.1.1 Coagulation and Flocculation

Coagulation-flocculation typically acts as a pre-treatment process for the sedimentation and filtration process in order to improve the removal of particles in the treatment process. Coagulation and flocculation happen in consecutive steps. During the coagulation and flocculation, the particles collide and form floc. Incomplete coagulation will lead to the failure of flocculation, hence reduces the effectiveness of the sedimentation and filtration process.

Coagulation is a process which a gelatinous mass is produced due to the neutralization of charges. The larger mass is formed and settled or trapped in the filter. In the coagulation process, coagulant such as aluminium sulphate is added to the water. The coagulant which has the opposite charges of the suspended solid neutralize the negative charges of the suspended solid. This enable the small suspended particles to stick together and form slightly larger particles (microflocs) which cannot be seen by naked eye. A high energy and rapid mixing is needed to disperse the coagulant properly, enhance the collision of particle and prevent incomplete coagulation (Minnesota Rural Water Association, n.d.).

Flocculation is the process to increase the particle size of microflocs to visible suspended solid through gentle mixing. Collision of microflocs particles lead to formation of larger pinflocs. Further collisions and interaction with the coagulant increase the floc size to form macroflocs. Sedimentation can be done when the optimum size and strength of macroflocs is achieved. Flocculation

requires longer operational time compared to coagulation. More careful attention is needed for the mixing velocity and energy to prevent tearing or shearing of floc (Minnesota Rural Water Association, n.d.).

2.1.2 Biodegradation

Biodegradation is a process which the structures of compounds are changed by the microorganisms through the metabolic and enzymatic action. In biodegradation process, microorganisms such as bacteria and fungi decay the hazardous organic waste materials. Degradation of the waste materials converts these hazardous and poisonous contaminants into the secondary metabolites or degradation products which are less toxic and hazardous. The secondary metabolites are then turned into the nutrient or energy which further break down the remaining contaminants.

For the biodegradation to occur, some conditions have to be fulfilled. First, suitable microorganisms must be present with an energy source and nutrient which is required for the maintenance and growth of organisms. Besides, a carbon source and electron acceptor such as oxygen or carbon dioxide are required. Next, to make the biodegradation success, a suitable environmental condition including suitable temperature, pH and salinity levels is required.

There are two types of biodegradation, which are aerobic and anaerobic biodegradation. Aerobic biodegradation is the degradation in the presence of oxygen. In aerobic process, the organic contaminant is oxidized by the oxygen which acts as electron acceptor. In other word, the oxygen is being reduced by the organic contaminant. Oxygen reduces the hazardous compound into less toxic compounds, causing production of carbon dioxide, water and mineral salts. This process is known as “mineralisation”. For anaerobic biodegradation which the oxygen is absent, organic chemicals or inorganic anions can be used to substitute oxygen as the electron acceptor. The denitrifying or other reducing conditions such as iron-reducing or sulphate reducing conditions are required (Eskander and Saleh, 2017).

Facultative pond has a combination of aerobic zone, facultative zone and anaerobic zone for biodegradation. Aerobic bacteria present at the top of the pond while the anaerobic bacteria present at the bottom zone. The zone between

the aerobic zone and anaerobic zone is facultative zone which is partly anaerobic and partly aerobic. This is due to the facultative bacteria presented in this zone can adapt to the varying condition of oxygen. Figure 2.1 indicates the zone of operation in a facultative pond (Department of Natural Resources & Environment - State of Michigan, 2010).

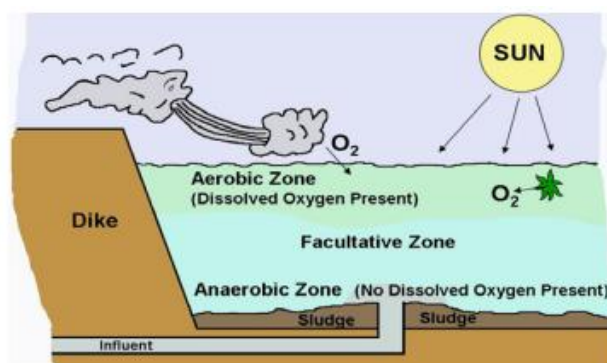


Figure 2.1: Zone of Operation in a Facultative Pond (Department of Natural Resources & Environment - State of Michigan, 2010)

2.1.3 Adsorption

Adsorption is a simple techniques used to remove organic and inorganic compounds from wastewater. When a substance accumulates at a surface or interface of another substance, it is known as adsorption. In the adsorption process, chemical species is removed from the fluid phases (gases or liquid) onto the solid surface. In the wastewater treatment, the contaminant molecules or ions are removed from the aqueous solution onto the surface of solid using adsorption. Adsorbent is the solid material with the adsorption sites. The species which are being adsorbed on the adsorption site of the adsorbent are known as adsorbate. When the adsorbed species are released back to the liquid after leaving the adsorption site, the process is known as desorption. Desorption occurs due to the varying properties of liquid phase such as temperature and pH. Figure 2.2 indicates the basic terms of adsorption (Worch, 2012). Adsorption is suitable to be used to treat the wastewater due to its capability to remove the hazardous substances which have small concentrations and are difficult to be removed by using traditional secondary treatment method.

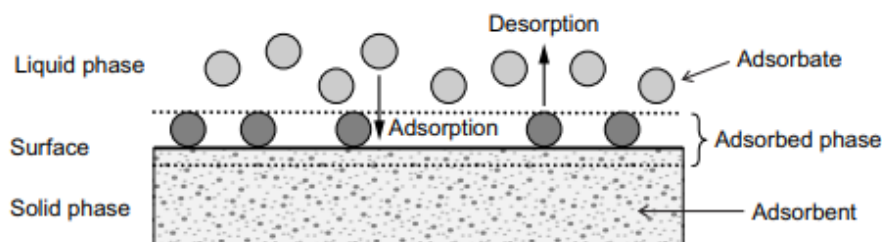


Figure 2.2: Basic Terms of Adsorption (Worch, 2012)

There are two types of adsorption depending on the interaction between the adsorbate molecules and adsorbent surface. The first type of adsorption is known as physisorption. Temporary electric dipoles interact with the permanent electric dipoles to produce interactive forces called van der Waals forces. Van der Waals forces alters the electronic arrangement of the molecules. Low activation energy (20 kJ-40 kJ) enable the single layer or multilayer adsorption to be occurred. In physisorption, desorption is occurred at a lower temperature due to the weak interaction forces of physisorbates. The second type of adsorption is known as chemisorption. Chemisorption occurs due to the chemical bond between the adsorbate and adsorbent. Compared to physisorption, chemisorption has higher activation energy (200 kJ-400 kJ). Therefore, only monolayer adsorption can be occurred. Unlike physisorption, chemisorption occurs at very high temperature (Adeleke et al., 2019).

The solid adsorbents have energetically heterogeneous surface. The solid adsorbent substances have different energies active adsorption site on their surface and specific electronic and spatial properties to enable their interaction with the adsorbates or solutes present in the adjacent aqueous phase. In the adsorption process, the surface areas of the adsorbents play an important role. Higher surface area indicates larger amount of active sites available for adsorption and therefore increases the efficiency of the adsorbents. Engineered adsorbents have high surface areas of 10^2 and 10^3 m^2/g due to their high porosity which increase the internal surface areas of the adsorbent. The external surface areas of adsorbents (typically < 1 m^2/g) are smaller than the internal surface areas and do not contribute much for the large surface area of adsorbent (Worch, 2012).

Activated carbon is one of the engineered adsorbents which are widely used in water treatment because the activated carbon is capable to remove the pollutants in wide spectrum. Besides, activated carbon is inert which the reaction between adsorbent and adsorbate can be prevented. Furthermore, activated carbon has high thermal stability. However, activated carbon has some disadvantages such as the slow adsorption kinetic and challenges to regenerate the adsorbents. Recently, carbon nanotubes (CNTs) have comparable efficiency compared to activated carbon due to their special properties. For example, CNTs have more tailored surface chemistry, higher adsorption capacity and faster equilibrium rates. Furthermore, the interaction between the adsorbents and adsorbates are stronger in CNTs. However, CNTs have smaller particle size that can lead to excessive pressure drop (Liu, Zhang and Pan, 2012).

Although the adsorbents such as activated carbon and carbon nanotubes have the high effectiveness to remove various pollutants from wastewater, however this conventional adsorption method possess some challenges such as high cost of adsorbent and difficulty in separation of the adsorbents from the solution. Hence, to segregate the spent adsorbent from the wastewater, use of magnetism can be applied to recover and regenerate the spent adsorbent effectively which leads to reduction of the capital cost. In the magnetic adsorption, magnetic particles such as oxides of Fe, Co, Ni and Cu embed on the base adsorbent such as activated carbon and CNTs to form a magnetic adsorbent. With the aid of external magnetic field, the spent magnetic adsorbents can be removed easily from the water as the metal component is presented in the adsorbent (Mehta, Mazumdar and Singh, 2015).

2.1.4 Fenton Process

The limitations and ineffectiveness of the conventional wastewater treatment methods had caused researchers to study and develop new technologies to treat the toxic organic pollutants. Advanced Oxidation Process (AOP) such as ozone oxidation, photochemical oxidation, Fenton oxidation has been applied widely in removing the organic matter by biodegrading the organic pollutants through oxidation. In AOP, hydroxyl radicals ($\bullet\text{OH}$) radicals are produced from oxidants such as hydrogen peroxide (H_2O_2), ozone or others. Among these oxidants,

Fenton process which uses hydrogen peroxide as oxidant is the most popular AOP method because of it can be applied in different application, easy to be operated and able to degrade and mineralize components rapidly (Zhang et al., 2019).

Fenton process was first developed by H.J.H. Fenton in 1894 and has been further studied by other researchers for long period. Researches claimed that there are more than 20 chemical reactions in Fenton process and for the conventional homogeneous Fenton process, the best pH range for the process is pH 2 to pH 4. Shen et al. (2017) had developed the reaction mechanisms of Fenton process with the rate constants at pH 4 as shown in Table 2.1 which the general core reaction is shown in Equation 2.1. Fenton reagents is a homogenous solution of iron ions and H_2O_2 . In the Fenton process, H_2O_2 reacts with Fe^{2+} ions to produce hydroxyl radical ($\bullet\text{OH}$) under operating conditions of low pH. The hydroxyl radical then degrades the organic pollutants to less hazardous carbon dioxide and water. The mechanism for the Fenton process is illustrated in Figure 2.3.

Table 2.1: Reaction Mechanism of Fenton Process and Corresponding Rate Constants at pH 4 (Shen et al., 2017)

Reaction	Rate constant, k ($\text{M}^{-1}\text{S}^{-1}$)	Equation
$\text{Fe}^{2+} + \text{H}_2\text{O}_2 \rightarrow \text{Fe}^{3+} + \bullet\text{OH} + \text{OH}^-$	5.5×10^1	2.1
$\text{Fe}^{3+} + \text{H}_2\text{O}_2 \rightarrow \text{Fe}^{2+} + \text{HO}_2\bullet + \text{O}_2\bullet^- + \text{H}^+$	2.5×10^{-3}	2.2
$\text{Fe}^{2+} + \bullet\text{OH} \rightarrow \text{Fe}^{3+} + \text{OH}^-$	3.2×10^8	2.3
$\text{Fe}^{2+} + \text{HO}_2\bullet / \text{O}_2\bullet^- \rightarrow \text{Fe}^{3+} + \text{H}_2\text{O}_2$	2.4×10^6	2.4
$\text{Fe}^{3+} + \text{HO}_2\bullet / \text{O}_2\bullet^- \rightarrow \text{Fe}^{2+} + \text{O}_2 + \text{H}^+$	7.7×10^6	2.5
$\text{H}_2\text{O}_2 + \bullet\text{OH} \rightarrow \text{HO}_2\bullet / \text{O}_2\bullet^- + \text{H}_2\text{O}$	3.3×10^7	2.6
$\bullet\text{OH} + \bullet\text{OH} \rightarrow \text{H}_2\text{O}_2$	5.2×10^9	2.7
$\bullet\text{OH} + \text{HO}_2\bullet / \text{O}_2\bullet^- \rightarrow \text{H}_2\text{O} + \text{O}_2$	7.5×10^9	2.8
$\text{HO}_2\bullet / \text{O}_2\bullet^- + \text{HO}_2\bullet / \text{O}_2\bullet^- \rightarrow \text{H}_2\text{O}_2$	1.4×10^7	2.9

However, the homogenous Fenton process has some shortcomings. The homogeneous Fenton Process has small range of operating pH due to

deactivation of iron species catalyst at high pH. Furthermore, formation of iron sludge (accumulation and precipitation of Fe^{3+} at above pH 3) occurs as the rate of oxidation of Fe^{2+} to Fe^{3+} (Equation 2.1) is much higher than reduction of Fe^{3+} to Fe^{2+} . Efficient cycling of Fe^{2+} and Fe^{3+} ions cannot be achieved. Formation of iron sludge causes the difficulty in iron sludge separation, decrease in catalytic activity and production of secondary waste, causing environmental issues (Zhang et al., 2019).

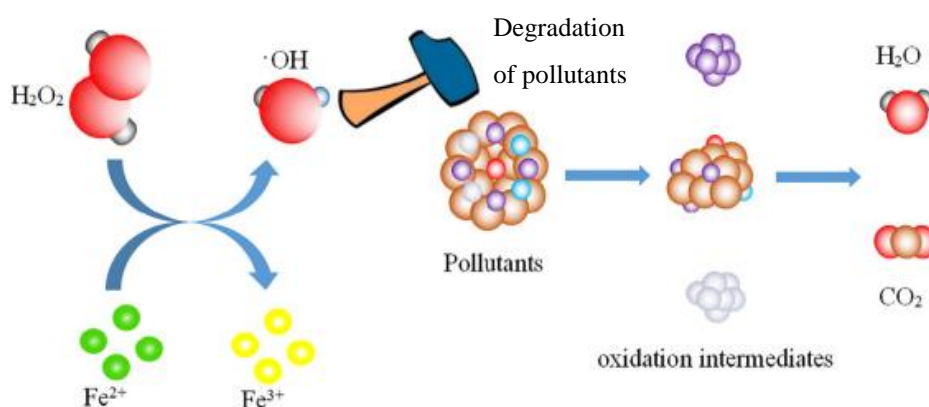


Figure 2.3: Reaction Mechanism for the Fenton process (Zhang et al., 2019)

To solve the shortcomings of homogenous Fenton Process, heterogeneous Fenton process is introduced. In the heterogeneous Fenton Process, solid catalyst which consist of catalytic active Fe^{2+} components are used instead of the catalyst Fe^{2+} in the homogeneous Fenton system. The reaction takes place at the active sites on the solid catalyst surface. This avoids leaching of iron ions and widens the operating pH range. The specific structure of the solid catalyst also helps to speed up reduction of Fe^{3+} to Fe^{2+} which enhances the cycling of Fe^{3+} and Fe^{2+} and reduces formation of iron sludge (Zhang et al., 2019). The mechanism for heterogeneous Fenton process is shown in Figure 2.4.

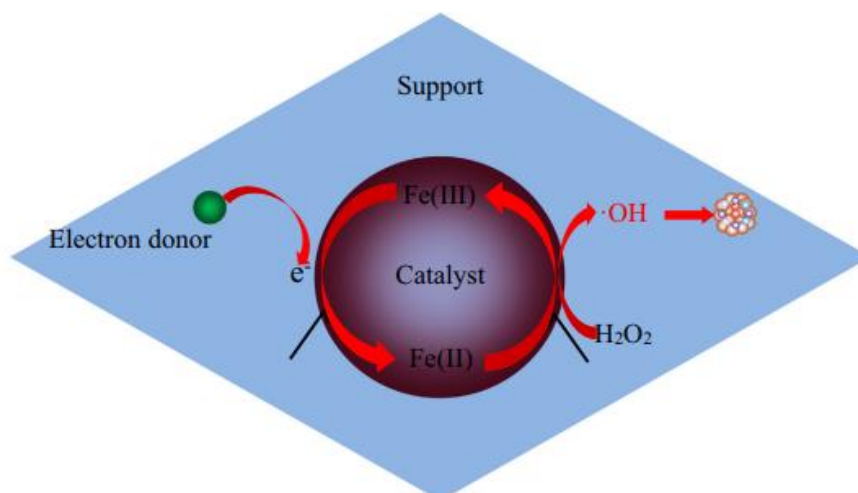


Figure 2.4: Mechanism for Heterogeneous Fenton Process (Zhang et al., 2019)

2.1.5 Comparison of Wastewater Treatment Method

The advantages and disadvantages of different wastewater treatment method are summarized in Table 2.2.

Table 2.2: Summary of Different Wastewater Treatment Method (Ramachandran et al., 2013)

Treatment Method	Advantages	Disadvantages
Coagulation and Flocculation	Easy to operate, low cost	Formation of sludge, difficulty to dispose waste, requirement of large amount of chemical to change pH
Biodegradation	Economically feasible, only relies on metabolic, generate biogas	Long-time operation environmental issues, frequent maintenance and nutrition provision are needed
Adsorption	High effectiveness, high capacity of adsorbents	Difficulty in separation, regeneration problem, production of secondary waste
Fenton process	No sludge formation, high effectiveness of degradation	Expensive, narrow working pH range, secondary disposal of the iron sludge

Adsorption and Fenton Process are methods which are very effective in the removal of contaminants from wastewater. However, both of these methods have their own disadvantages which limits their applications. Hence, simultaneous adsorption and degradation of contaminants is introduced to reduce the limitations of both methods. For instance, the thermal generation problem of carbon nanotubes can be substituted by the Fenton oxidation-driven regeneration. On the other hand, the iron sludge formation in the Fenton Process can be reduced by introducing the MMWCNTs which consist of Fe_3O_4 as catalyst. Simultaneous adsorption and degradation also helps to increase the available pH range of the reaction.

2.2 CNTs

2.2.1 General Introduction of Carbon Nanotubes

Carbon nanotubes (CNTs) are carbon tubes having relatively small diameters (a few nanometer), compared to the length of the tubes (up to a few micrometer). CNTs have hollow structures which consist of one or more walls. A carbon nanotube is a member of the fullerene structural family.

Before 1985, scientists and researchers considered that there were only two types of solid forms pure carbon which were diamond and graphite. However, Richard Smalley and Harry Kroto accidentally discovered Buckminster fullerenes, a third allotropic form of solid carbon. They used an extremely strong pulse to vaporize a graphite sample and the sample was analysed by mass spectrometer. The high peak of spectrum indicated the presence of carbon clusters corresponding to 60 carbon atoms, C_{60} . Later, C_{36} , C_{70} , C_{76} and C_{84} were also discovered. Hence, scientists and researchers were forced to change their conception of natural world. Buckminster fullerenes were recognized as a new carbon allotrope. Buckminster fullerenes, which are also known as buckyballs are ball-shaped molecules which are made up of sixty carbon atoms with an arrangement of icosahedral geometric structure resembling a soccer ball (Sarangdevot and Sonigara, 2015).

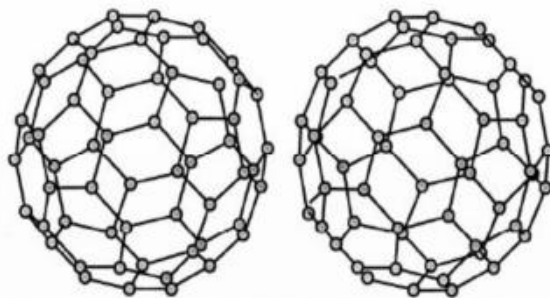


Figure 2.5: 3D Structure of the Buckminster Fullerene Molecule (Sarangdevot and Sonigara, 2015)

Iijima discovered carbon nanotubes in 1991. The structure of CNTs are formed by rolling and shaping the thin benzene ring carbon sheets into a perfect cylinder and at least one end of the CNTs are normally covered by buckyball structure. CNTs have small diameters and large lengths. The ratio of length to diameter is about 1000, therefore CNTs are considered to have a nearly one-dimensional structure. In the CNTs, each carbon atom connects to three neighbouring atoms, as in graphite. Hence, CNTs are considered as rolled-up graphene sheets. The sp^2 bonding structure in CNTs causes CNTs to have a stronger structure compared to diamond with sp^3 bonds (Sarangdevot and Sonigara, 2015).

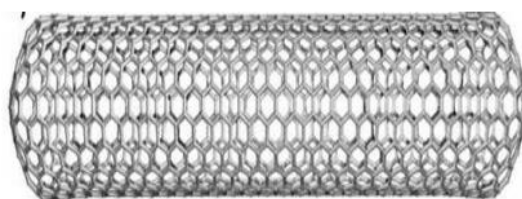


Figure 2.6: Structure of Carbon Nanotube (Sarangdevot and Sonigara, 2015)

CNTs have specific strength due to the presence of sp^2 bonds. CNTs can combine together, replacing some sp^2 bonds by sp^3 bonds under high pressure to form unlimited length strong wires. The outstanding properties of CNTs cause them to be used widely in different application. CNTs have good mechanical, thermal and chemical properties compared to other components. For example, CNTs are very strong in axial direction with Young's modulus lies between 270 GPa to 950 GPa. Besides, CNTs have significant quantum

effects although they have very small diameter. The good thermal conductivity of CNTs indicates the direct prove of 1-D quantization of phonon band structure in the nanotubes. The thermal conductivity of a material can be increased by a factor of 2 when only 1 % loading of pristine and functionalized nanotubes are added to different materials. However, the thermal properties of CNT depends on several factors including the amount of phonon-active modes, the distance of the free path for the phonons, and boundary surface scattering (Khan and Saeed, 2013).

In general, there are two types of carbon naotubes which are single-walled carbon nanotubes (SWCNTs) and multiwalled carbon nanotubes (MWCNTs). Both of them have their advantages and are used in different applications. SWCNTs and MWCNTs will be discussed in detailed in the following section.

2.2.2 Single-walled Carbon Nanotubes (SWCNTs)

Single-walled carbon nanotube (SWCNTs) can be described as tubes which is formed by perfectly rolling up a strip cut from an infinite graphene sheet as shown in Figure 2.7.

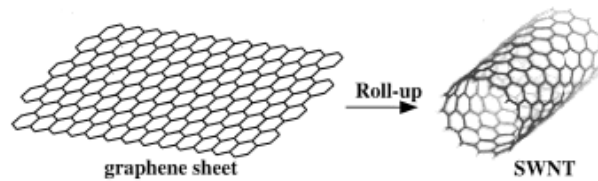


Figure 2.7: Formation of SWCNT from a graphene sheet (Wang, Huang and Lieber, 2002)

SWCNTs have typical diameters of 0.8 to 2 nm. Every SWCNT can be represented by a chiral vector which is defined as the vector Equation 2.10:

$$C_h \equiv na_1 + ma_2 \equiv (n, m) \quad (2.10)$$

where a_1 and a_2 are the graphene lattice vectors and n and m are integers. The chiral vector specifies the two graphene sheet atom which are identified when

the tube is formed (Wang, Huang and Lieber, 2002). The single-walled carbon nanotubes can be classified into three categories according to the relationship between n and m as shown in Table 2.3. Different structure of the SWCNTs possess different properties for their electronic structure, optical properties and dispersion of phonon.

The single-walled carbon nanotubes can have metallic or semiconducting characteristic depending on their chiral vector. If $(n-m)/3$ of the SWCNTs is an integer, the tubes have a metallic property. On the other hand, the SWCNTs are semiconducting material if $(n-m)/3$ is not an integer (Wang, Huang and Lieber, 2002).

One of the main characteristics of single-walled carbon nanotubes is their electric properties that are not exhibited by MWCNTs. The band gap of SWCNTs ranges from zero to 2 eV whereas MWCNTs are zero gap metal. The excellent electric properties cause SWCNTs to be used in a wide variety of application. For instance, SWCNTs can be used as nanoprobe for resonant tunnelling devices such as scan tunnelling microscope and atomic force microscopy. Besides, SWCNTs can be used as interconnects between device elements. For the semiconducting SWCNTs, they can be used to make nanometer-sized field-effect transistors. Finite-sized SWCNTs can be utilised to increase the operating temperature of nanotube-based devices. Last, the conductivity of the SWCNTs at low energies can be improved by adding magnetic impurities to the metallic nanotubes (Wang, Huang and Lieber, 2002).

Table 2.3: Classification of SWCNTs (Nanot et al., 2013)

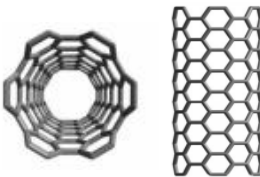
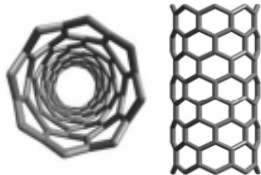
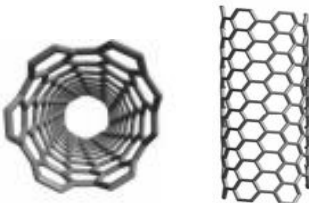
Categories	Chiral Vector
Armchair Nanotubes	$n = m$; Ch = (n, n)
	

Table 2.3 (Continued)

Categories	Chiral Vector
Zig-zag Nanotubes	$m = 0; Ch = (n, 0)$
	
Chiral nanotubes	$n \neq m \neq 0$
	

2.2.3 Multiwalled Carbon Nanotubes (MWCNTs)

Multiwalled carbon nanotubes (MWCNTs) are hollow carbon tubes made up of several rolled layers of graphene with sp^2 bond. The MWCNTs have long length that can grow several cm long with the diameters ranges from 3 to 30 nm. Hence, MWCNTs have a very high ratio of length to diameter, range from 10 to 10 million (Kukovecz, Kozma and Kónya, 2013). The structure of MWCNTs is indicated in Figure 2.8.

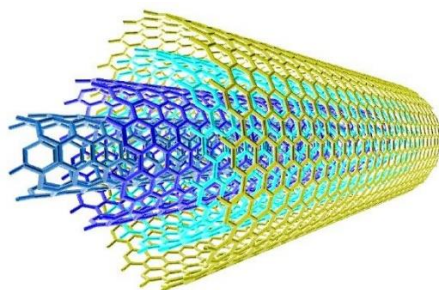


Figure 2.8: Structure of MWCNTs (Rafique et al., 2015)

Due to the constant wall thickness along the axis, MWCNTs have straight inner passage. The passage is not directly approachable to outside due to the covering of the end of MWCNTs by half fullerene spheres. However, to

access to the passage, different method such as oxidation, milling or ion beam treatment can be applied to open the nanotube. MWCNTs are still considered as 1-D form of carbon, but the specific properties that present in SWCNTs is not that significant in MWCNTs due to the higher dispersability of MWCNTs and the higher probability of the occurrence of defects. There are two models to explain the structures of MWCNTs which are Parchment model and Russian model. In Parchment model, a parchment scroll or rolled newspaper shape is formed by rolling only a single sheet of graphite around itself. In Russian Doll model, MWCNTs are formed by arranging multiple graphite sheets into concentric cylinders (Alsharif, Taha and Khan, 2017). The schematic draft of the layer arrangement of Parchment model and Russian model are shown in Figure 2.9 (A) and (B) respectively.

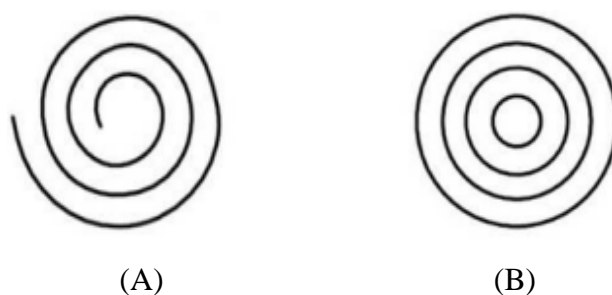


Figure 2.9: Schematic Draft of the Layer Arrangement of (A) Parchment Model and (B) Russian Model (Jurková, 2013)

To distinguish multiwalled carbon nanotubes with single-walled carbon nanotubes, the diameter and Raman spectrum of the carbon nanotubes can be used as a basis. MWCNTs have larger diameter (3 to 30 nm) compared to SWCNTs (0.8 to 2 nm). Comparing their Raman spectrum, the diameter distribution of nanotubes in SWCNTs can be identified easily by measuring radial breathing mode (RBM). However, RBM signal is weaker and more difficult to be observed in MWCNTs compared to SWCNTs due to ensemble of carbon nanotubes with a very wide range of carbon nanotubes diameter in MWCNTs and broadening of diameter signal due to the ensemble average inner tubes diameters (Costa et al., 2008). SWCNTs are more flexible while MWCNTs are stiffer and more rigid. To differentiate MWCNTs with carbon nanofiber (CNF), MWCNTs have as many large molecules as the amount of

their walls but CNF has many graphitic platelets which are smaller than the fiber, bonded together by secondary bonding forces with different arrangements (Kukovecz, Kozma and Kónya, 2013).

MWCNTs have very low solubility in all liquid. Hence, “solution” term should not be used for MWCNTs. There are several ways to improve MWCNTs dispersions such as decrease in length of carbon nanotubes, functionalization of surface and application of surfactant molecules. MWCNTs have high surface area. The open MWCNTs consists of empty spaces for the adsorption governed by capillary condensation. Hysteresis-free adsorption-desorption profile can be observed in MWCNTs with one open end. In general, MWCNTs are considered as mesoporous materials. MWCNTs have mesoporous volume of 0.5-2.0 cm³/g. For the mechanical properties of MWCNTs, MWCNTs have Young’s modulus in TPa range and 60 GPa tensile strength. MWCNTs have effective average thermal conductivity of 200 W/(m K) (Kukovecz, Kozma and Kónya, 2013).

MWCNTs can be used in the adsorption, filtration and membranes for the waste treatment. MWCNTs can be used together with membrane technology for the excellent filtration/adsorption abilities of MWCNTs and lower cost. For example, low nanotube coverages of MWCNTs coated with the cellulose fiber filter are able to filter out more than 99% of airborne fine particles. MWCNTs can also improve the selectivity of adsorption by enhancing the affinity of nanotube membrane towards a particular molecule through covalent functionalization. Furthermore, MWCNTs can be used as a support for heterogeneous catalysis because of their high specific surface area and heat stability. MWCNTs are better supports compared to conventional porous supports such as silica and carbon black due to absence of bottled pore or dead ends, hence all the surface of nanotube can be utilized for the reaction. Besides, the pressure drop on the catalyst bed can be reduced and the space velocities can be increased. The other applications of MWCNTs includes nanotube heat sinks, heat-conductive polymer nanocomposites and temperature sensor due to their good thermal conductivity (Kukovecz, Kozma and Kónya, 2013).

2.2.4 Comparison of Single-walled Carbon Nanotubes and Multiwalled Carbon Nanotubes

Some of the comparison between single-walled carbon nanotubes and multiwalled carbon nanotubes are shown in Table 2.4.

Table 2.4: Comparison of Single-walled Carbon Nanotubes and Multiwalled Carbon Nanotubes (Sarangdevot and Sonigara, 2015)

	SWCNTs	MWCNTs
Layer of graphene	Single	Multiple
Catalyst	Required for production	Not required
Bulk synthesis	Harder due to proper control over atmospheric condition is required	Easier
Purity	Low	High
Chance of defect	High during functionalization	Low, but once happens it is harder to improve
Accumulation in body	Low	High
Characterization	Easier	Complex structure
Ease to twist	High	Low

2.3 Synthesis of Magnetic Multiwalled Carbon Nanotubes (MWCNTs-Fe₃O₄) by Direct Doping Method

Direct doping method is an easy way to decorate magnetic nanoparticle on the carbon nanotubes. The method involves the addition of a solution containing positively charged Fe₃O₄ to a solution consisting negatively charge carbon nanotube. To make this happen, carbon nanotubes must be first functionalized chemically with carboxylate group. Chemical functionalization of CNTs by covalent and non-covalent bonding enhances their dispersion in liquid phase as well as the polymer matrices. The most common method to produce carboxylate group on the surface MWCNTs (MWCNTs-COOH) is to reflux and oxidize MWCNT in the acid medium such as concentrated nitric acid (HNO₃) (Cheng et al., 2008). Other method to functionalize MWCNT includes using a radical polymerization initiator, 4,49-azobis (4-cyanovaleric acid) (V501) instead of

refluxing in concentrated HNO_3 to produce alkyl radicals consists of carboxylate (COO^-) (Stoffelbach et al., 2005).

Then, magnetic nanoparticles are added to solution consist of functionalized MWCNT at an appropriate pH. Functionalized carbon nanotubes and the magnetic nanoparticles have different pH_{pzc} . At the pH lower than the pH_{pzc} , the species have a positive charge. The species have a negative charge when the pH is higher than pH_{pzc} . Difference of the pH_{pzc} will results in the opposite charge of the magnetic nanoparticles and functionalized MWCNT at certain pH. Magnetic nanoparticles will have a positive charge while the carbon nanotubes will have a negative charge. Hence, the negatively charged magnetic nanoparticles are attracted to the positively charged functionalized MWCNT, forming a magnetic Fe_3O_4 doped multiwalled carbon nanotube, MWCNTs- Fe_3O_4 . The schematic diagram of synthesis of MWCNTs- Fe_3O_4 by using V501 initiator to functionalize MWCNT is illustrated in Figure 2.10.

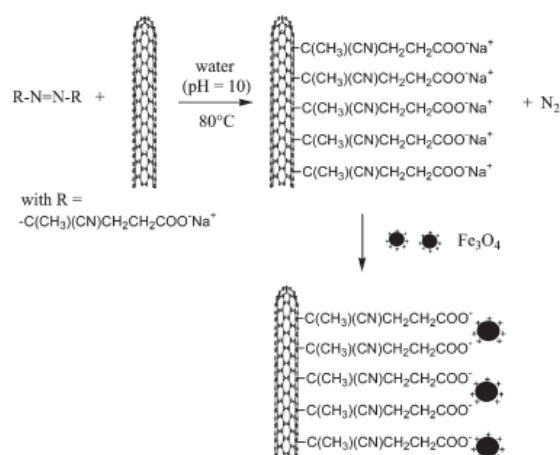


Figure 2.10: Schematic Grafting of CNTs and Decoration by Fe_3O_4 Nanoparticles (Stoffelbach et al., 2005)

2.4 Characterization Study

2.4.1 Fourier Transform Infrared Spectroscopy (FTIR)

FTIR is a rapid technique that provides the measurement of whole spectra accurately. It is used to determine the adsorbed species and to study how these species are chemisorbed on the surface of other species. Molecules vibrate and alter the dipole moment of the molecules. They become IR active and the light

of a specific wavelength is absorbed. The absorption of this specific wavelength is then translated to indicate the specific bond of a molecule (Wang, Wang and Zhou, 2017).

FTIR can be used to confirm the composition of MWCNTs-Fe₃O₄. Zhou et al. (2014) used FTIR with KBr pellet technique. Their studies claimed that peak at 582 cm⁻¹ indicated Fe-O-Fe stretching vibration of Fe₃O₄. Study by Wang et al. (2014) also claimed that 442 cm⁻¹ in the FTIR spectrum indicated presence of Fe₃O₄ magnetic nanoparticles. Zhou et al. (2014) also reported that peak at 3438 cm⁻¹ represented O-H stretching of MWCNTs, proving that large amount of carboxyl and hydroxyl groups were present on the surface of MWCNTs.

2.4.2 X-Ray Diffraction (XRD)

XRD is a rapid analytical method to study the phase of a crystalline material. The information on dimensions of unit cell can be also obtained using XRD. The working principle of XRD can be related to a crystalline sample and X-rays' constructive interference. Constructive interference and a diffracted ray are formed when incident X-rays interact with the sample. Bragg's Law ($n\lambda = 2d \sin \theta$) illustrates derivation of lattice spacing through diffraction of X-rays by crystal planes (Dutrow and Clark, 2019). The average crystal size can be calculated using Scherrer's Equation (Equation 2.11).

$$L = \frac{K\lambda}{\beta \cos \theta} \quad (2.11)$$

where L = average crystalline size (Å)
 K = constant, normally 0.9
 λ = X-ray wavelength (nm)
 β = peak width of the diffraction peak profile at half maximum height resulting from small crystallite size (radians)
 θ = the angle between the beam and the normal to the reflecting plane (degrees)

Some studies are taken as reference in determining the operating condition of XRD. Wang et al. (2014) used XRD-3 X-ray diffractometer with nickel filtered Cu K α radiation ($\lambda = 0.15406$ nm). The current used was 20 mA and voltage was 36 kV. It had a scanning rate of 4 °/min with 2θ ranged from 5 ° to 80 °. XRD could be utilised to study composition of crystalline structure of MWCNTs-Fe₃O₄ and XRD pattern of Fe₃O₄ nanoparticle. Average size of Fe₃O₄ could also be determined.

According to Wang et al. (2014), peak exhibited at $2\theta = 25.8$ ° corresponded to (002) plane indicated the hexagonal graphite structure of MWCNT whereas the highest peaks at 2θ values of 18.2 ° (111), 30.0 ° (220), 35.3 ° (311), 42.9 ° (400), 53.4 ° (422), 56.9 ° (511) and 62.5 ° (440) were related with characteristic peaks of cubic phase Fe₃O₄ magnetic nanoparticles.

2.4.3 Scanning Electron Microscope Coupled with Energy Dispersive X-Ray (SEM-EDX)

A focused beam of high-energy electrons is generated by SEM to produce different signals. The signals produced are able to provide useful information regarding the samples such as morphology (texture), chemical composition, crystallographic and orientation of the materials (Swapp, 2019). EDX is coupled with SEM to analyse the elements and their proportion at different location are estimated. Sample's overall mapping can be obtained (Joshi, Bhattacharyya and Ali, 2008).

SEM can be used to investigate the morphology of MWCNTs-Fe₃O₄ nanocomposite. According to Rahmawati et al. (2017), MWCNTs existed in bundles structure. The defect on surface of MWCNTs could be used by Fe₃O₄ as nucleation sites. For Fe₃O₄ morphology, the Fe₃O₄ nanoparticles adhered together and form spherical clusters, with size ranged from 10 to 20 nm individually. For the morphology of MWCNTs-Fe₃O₄ nanocomposites, Fe₃O₄ were interwoven by MWCNTs network. Fe₃O₄ binded on the surface of MWCNT. Besides, Fe₃O₄, in a structure of large agglomeration also presented as free particles in MWCNTs-Fe₃O₄, due to smaller amount of MWCNTs to provide growth and nucleation sites for Fe₃O₄. By coupling EDX with SEM, the elemental composition of the nanocomposite can be identified.

2.4.4 Brunauer–Emmett–Teller (BET)

Surface area is one of the important properties to characterize because it is one of the factors which will affect the catalytic activity. The smaller the particles, the higher the surface area of the catalyst and this can lead to higher catalytic activity. To measure the surface area of solid or porous catalyst, Brunauer–Emmett–Teller (BET) theory can be applied. BET analysis can be used to determine the specific surface area and distribution of pore size. The analysis is performed by adsorption and desorption of non-reactive gas molecules such as N₂ molecules on the surface of catalyst when the pressure differs. The amount of gas molecules being adsorbed on the catalyst increases as the pressure increases and eventually form a monolayer which cover the entire surface of catalyst. Desorption occurs when pressure decreases. The isotherms are then transformed to linearized BET plot in order to identify the monolayer loading (Sinha et al., 2019). The relationship between the amount of gas molecules being absorbed and relative pressure can be explained by BET equation (Equation 2.12).

$$\frac{1}{X\left[\left(\frac{P_0}{P}\right) - 1\right]} = \frac{1}{X_m C} + \frac{C - 1}{X_m C} \left(\frac{P}{P_0}\right) \quad (2.12)$$

where X = number of gas molecules adsorbed
 X_m = number of gas molecules adsorbed as monolayer
 P/P_0 = relative pressure
 C = BET constant

According to Moazzen et al. (2019), MMWCNTs had higher surface area than the pristine MWCNTs. This might because of the increasing pores number, reduction of particles size or increasing crystal defects that increase the active sites.

2.4.5 Thermogravimetric Analysis (TGA)

Thermogravimetric analysis is a characterization technique to analyse thermal stability of a sample. This analysis can also be used to determine the fraction of

volatile components in the sample. In the analysis, the mass change is observed during the heating of sample in air or inert condition such as helium or argon at a constant rate (Rajisha et al., 2011). The mass of sample is measured as the sample temperature is increased. During heating, the sample may lose material or react with surrounding atmosphere due to some factors such as evaporation of volatile components, oxidation of metals, oxidative or thermal decomposition. This lead to the mass change (lost or gain mass) of sample and eventually production of steps in TGA curve or peaks in differential thermogravimetric (DTG) curve (Bottom, 2008).

According to Sadegh, Shahryari-ghoshekandi and Kazemi (2014), iron oxide had stable thermal stability between 0 °C to 1000 °C. The increase of mass at wide range of temperature was due to the oxidation of Fe_3O_4 to Fe_2O_3 . For the pristine MWCNTs' TGA curve, water and functional group were removed from sample at lower temperature causing a small mass loss being observed. At higher temperature (635 °C to 730 °C), nanotubes oxidized and led to obvious weight loss. For functionalized MWCNT (MWCNT-COOH), weight loss started at 150 °C, indicating the decomposition of carboxylic acid and hydroxyl groups functional group. The MWCNT-COOH had better thermal stability than pristine MWCNT because MWCNT-COOH played a role as radical scavengers and chain traps in both cleaving of chain and formation of radical, slowed down the thermal degradation (Kong, Ahmad and Shanks, 2016). For MWCNTs- Fe_3O_4 , weight loss occurred at lower temperature range (490-635 °C), leaving iron oxide residue weight. This showed that metal oxide nanoparticles had important catalytic role in oxidation of carbon (Sadegh, Shahryari-ghoshekandi and Kazemi, 2014). Besides, doped MWCNTs- Fe_3O_4 could improve the thermal stability of catalysts due to barrier of nanoparticles to heat permeability into the catalyst, hence decreased the diffusivity of less volatile decomposition products (Kong, Ahmad and Shanks, 2016).

2.4.6 UV-visible (UV-vis) Spectroscopy

In UV-vis spectrophotometer, a sample of compound is exposed to UV light from a light source such as a Xenon lamp to obtain the UV-visible spectrum of the analysed compound. From the UV-visible spectrum, one can determine what

wavelength of light are being absorbed. The higher value of absorbance indicates the larger amount of a particular wavelength is being absorbed (Joshi, Bhattacharyya and Ali, 2008). The concentration of a component can be related to the absorbance according to Beer-Lambert Law which claims that absorbance is proportional to concentration of substance in solution (RSC, 2009). The Beer Lambert Law is indicated in Equation 2.13.

$$A = \varepsilon cl \quad (2.13)$$

where A = absorbance
 l = dimension of the cell or cuvette (cm)
 c = concentration of solution (mol dm⁻³)
 ε = constant for a particular substance at a particular wavelength (dm³ mol⁻¹ cm⁻¹)

According to Abdel Salam, Gabal and Obaid (2012), amount of aniline adsorbed could be determined by using UV-vis spectrophotometer. Aniline concentration was determined by using UV-vis spectrophotometer at a wavelength of 230 nm. According to Ilic et al. (2000), absorption band of aniline occurred at 280 nm.

2.5 Parameter Study

2.5.1 Effects of Solution pH

Both adsorption and Fenton process are affected by the solution pH. In adsorption, the adsorption efficiency can be affected by pH because pH alters the electric charge of the adsorbent surface and the ionization degree of aniline. According to Baneshi et al. (2017), the optimal pH for the bio-adsorption of aniline using dried activated sludge was pH 6. At pH lower than the pH_{pzc} , the adsorbent species had a positive charge. The species had a negative charge when the pH was higher than pH_{pzc} . The pH_{pzc} of the activated sludge was 6.7. Hence in the optimal pH (pH 6) which the pH was lower than pH_{pzc} , it had a positive charge which enable it to adsorb aniline which is a weak base. According to Li

et al. (2015), the pH_{pzc} for MWCNTs- Fe_3O_4 is pH 3.8 while according to Khan, Nazir and Khan (2016), the pH_{pzc} of MMWCNTs is ~ 4.3 . The negative base-10 logarithm of the acid dissociation constant, pKa is also a factor which have to be considered when identifying the optimal pH. The reaction between aniline and H^+ ions in the acidic medium converts aniline to anilinium ions with positive charge and pKa of 9.37. At pH lower than pKa, aniline can be protonated to produces positive ions. When pH is higher than pKa, aniline is neutral or negatively charged. Hence at highly acidic medium, aniline produce positive ions which repel with the H^+ ions in medium, reducing the adsorption efficiency.

The importance of pKa can also be seen in report of Al-Johani and Salam (2011). The study reported that the pKa of aniline was 4.6. Hence, in the aniline adsorption by MWCNT, the adsorption efficiency in medium with pH 3 was very low due to electrostatic repulsion between the both positively charged aniline and carbon nanotubes. From pH 3 to 5 which was higher than the pKa, the efficiency of the adsorption increased to 80% for MWCNT 10–20. The efficiency dropped to 74% at higher pH (pH 8) because both MWCNT and aniline were negatively charged at pH 8. According to Abdel Salam, Gabal and Obaid (2012), pKa of aniline was 5.2 and optimum pH for adsorption of aniline occurred at pH 6. At lower pH, both aniline and MWCNTs/ferrite were positively charged. At higher pH, both aniline and adsorbent were negatively charged. Both of these condition enhanced the electrostatic repulsion and reduced the adsorption efficiency.

For homogeneous Fenton process, pH is a significant parameter that affects the degradation rate of aniline. According to Muruganandham et al. (2014), the optimum pH for general case of homogenous Fenton oxidation ranged from pH 2.8 to pH 3. Below this range, production of reactive hydroxyl radicals was lower due to production of $(\text{Fe}(\text{II}) (\text{H}_2\text{O}))^{2+}$ that reacted more slowly with hydrogen peroxide. Fe^{3+} was inhibited to be reacted with hydrogen peroxide at very low pH due to the scavenging effect of hydroxyl radicals by hydrogen ions. At pH exceeding pH 3, degradation rate decreased due to reduction of amount of free iron species. At pH higher than pH 3, inhibition of ferrous ions production occurred due to precipitation of Fe^{3+} to form ferric oxyhydroxides and H_2O_2 was broken down to H_2O and O_2 .

For heterogeneous Fenton process, a wider range of working pH can be used. According to Liu et al. (2016), removing aniline by the heterogeneous Fenton's reaction with Ni-Fe oxalate complex catalyst had optimal initial pH of 5.4. However, the catalyst had a good pH tolerance property to degrade the aniline effectively with a wide initial pH from 3 to 8. Besides, study of Wang et al. (2014) in removal of MB in a Fenton-like reaction using MWCNTs-Fe₃O₄ as catalysts reported that there was only a small change in MB removal efficiency varied from 88.13% to 98.68%, when the solution pH differed from pH 1 to pH 10. Hence, the effect of pH in heterogeneous is not as significant as it is in homogeneous Fenton process.

2.5.2 Effects of Temperature

Temperature is considered as a factor that affects the removal efficiency of aniline in adsorption and Fenton degradation. Both adsorption and degradation of aniline is usually done at a lower temperature which is room temperature. For example, Kakavandi et al. (2013) had studied about the effect of temperature on adsorption of aniline using Fe₃O₄-activated carbon magnetic nanoparticles. In the study, it could be seen that the adsorption efficiency decreased with increasing temperature. For the aniline with initial concentration of 50 mg/L, the adsorption efficiency decreased from 99.9% to 84.4% when the temperature increased from 20 °C to 50 °C. The adsorption capacity also decreased from 25 to 21.1 mg/g in this range of temperature. The similar trend could be observed in the study by Abdel Salam, Gabal and Obaid (2012). Their report claimed that in the aniline adsorption by using MWCNTs/ferrite nanocomposite, the adsorption efficiency decreased from 99.1% to 66.3% when the temperature was raised from 15 °C to 45 °C. The low optimum temperature indicated that the adsorption of aniline was an exothermic process.

For the degradation of aniline using Fenton reagent, most of the process were carried out at low temperature, usually at room temperature. For example, all the preparation and experiments for aniline degradation by Fenton process were conducted at room temperature in the study by Ratanatamskul, Masomboon and Lu (2011). Liu et al. (2016) reported that the rate constant for aniline degradation through heterogeneous Fenton's reaction by utilizing a Ni-

Fe oxalate complex catalyst increased from 0.055 to 0.22 min⁻¹ when the temperature was increased from 10 °C to 30 °C which fulfilled the agreement of reaction rate increases by 2 to 4 times when the temperature is increased by 10 K (10 °C).

2.5.3 Effects of Initial Concentration of Aniline

Adsorption of aniline on the adsorbent depends on the initial concentration of aniline. Kakavandi et al. (2013) had studied about the effect of varying the initial concentration of aniline on the aniline removal efficiency using 2 g/L Fe₃O₄-activated carbon magnetic nanoparticles as adsorbent. The report showed that when the concentration of initial aniline increased from 50 to 300 mg/L, the removal efficiency after 5 hours decreased from 100 % to 58 %. In Baneshi et al. (2017)'s study on bio-adsorption of aniline using dried activated sludge, the removal efficiency after 2 hours reduced from 100 % to less than 20% with increasing initial aniline concentration from 50 mg/L to 250 mg/L. The similar trend was shown in report by Al-Johani and Salam (2011) that the adsorption efficiency after 30 minutes decreased from 64 % to 36% when aniline concentration was varied from 10 mg/L to 100 mg/L by using MWCNT 10-20 as adsorbent. All these trends prove that the adsorbent has limited number of active sites at high concentration of aniline. The adsorbent becomes saturated with aniline and the tendency for adsorption sites to remove the aniline efficiently decreases. However, adsorption capacity increases with increasing initial aniline concentration. This is because the mass transfer rate will increase with increasing initial aniline concentration. This speeds up the channelling of aniline from solution towards the liquid around the adsorbent, and eventually towards the adsorbent's surface (Baneshi et al., 2017).

For the Fenton process, the degradation of aniline is also affected by the initial concentration of aniline. For example, Ratanatamskul, Masomboon and Lu (2011) claimed that aniline degradation efficiency decreased from 100 % to 60 % after 2 hours when the initial aniline concentration was increased from 0.5 mM to 5 mM. This might be due to insufficient hydroxyl radical to degrade the aniline due to increment of amount of aniline molecules. According to Anotai, Lu and Chewprecha (2006), there was a reduction in the degradation efficiency

of aniline in Fenton oxidation from 52.2 % to 20.9 % when the aniline concentration was raised from 0.005 M to 0.05 M. The effect of pollutant concentration can be further proved by the study by Amritha and Manu (2016) which the removal efficiency decreased from 90 % to about 75 % with the increase of the initial concentration of 2-nitroaniline. The study claimed that this situation occurred due to the production of intermediate compound during oxidation that inhibited the availability of hydroxyl radical for oxidation process.

2.5.4 Effects of MWCNTs-Fe₃O₄ dosage

Both the magnetic adsorption and heterogeneous Fenton process are affected by the dosage of magnetic nanocomposite. Increasing the adsorbent can increase the pollutant removal efficiency. In Kakavandi et al. (2013) study, increasing the adsorbent (Fe₃O₄-activated carbon magnetic nanoparticles) dose from 0.5 to 2 g/L, there was a big improvement on the aniline removal efficiency after 5 hours, from 37.2 % to 100 %. Abdel Salam, Gabal and Obaid (2012) had studied the adsorption of aniline using MWCNTs/ferrite nanocomposite as adsorbent. The similar results were obtained. The removal efficiency increased from 22.4 % to 95.1% after 10 minutes with adsorbent dosage of 10-100 mg/20 ml solution. However, there was no significant change of efficiency when the adsorbent dosage was increased above 100 mg/20 ml solution. With adsorbent dosage of 130 and 150 mg/20 ml solution, 100% removal efficiency was achieved. This was due to initially increasing the adsorbent dosage increased the amount of active sites available for aniline adsorption. The less significant change in efficiency at higher dose could be explained by the adsorption of all adsorbate molecules on the adsorption site where 100 % removal efficiency was achieved.

MWCNTs-Fe₃O₄ dosage is also important for degradation process as varying dosage of Fe₃O₄-MWCNTs also alters the concentration of Fe₃O₄ which plays an important role in the Fenton Process. In general, increasing the dosage of Fe₃O₄ will increase the degradation efficiency. The effect of concentration of Fe₃O₄ can be seen from several studies. For example, results in study by Wang et al. (2013) showed that decomposition of H₂O₂ into hydroxyl radicals was difficult without the use of Fe₃O₄ because Fe₃O₄ played a role as catalyst to speed up the decomposition of H₂O₂ to reactive radicals. Phenol degradation had

a significant increase with the increase of Fe_3O_4 dosage from 0.2 to 1.0 g/L. Further increase of Fe_3O_4 dosage lowered the degradation efficiency due to the reduction of unit surface adsorption of H_2O_2 by excess Fe_3O_4 .

2.5.5 Effects of H_2O_2 Dosage

The adsorption of pollutant is not affected by the dosage of H_2O_2 . However, dosage of H_2O_2 plays an important role in affecting Fenton process. In general, increasing the dosage of H_2O_2 will increase the mineralization and degradation efficiency of the pollutant. However, the excessive dosage can bring a negative impact on the degradation efficiency. Wang et al. (2013) and Jia et al. (2019) used Fe_3O_4 as catalyst in Fenton process to degrade phenol and methyl orange respectively. Both their studies on the effect of H_2O_2 dosage had shown similar result which the degradation efficiency increased with the H_2O_2 dosage until certain point of dosage. Beyond the dosage, the degradation of the pollutants decreased.

Zhou et al. (2014) had studied on the effect of H_2O_2 dosage on the removal of tetrabromobisphenol A. (TBBPA) using MWCNTs- Fe_3O_4 in a heterogeneous Fenton reaction. When the H_2O_2 dosage was increased from 27 mmol/L to 54 mmol/L, the removal efficiency had a great improvement which the TBBPA residues was decreased from 9.7 to 5.3 %. This was due to increasing the H_2O_2 dosage increased the generation of $\bullet\text{OH}$ radicals to help in the oxidative degradation. However, further increase of dosage did not have significant improvement in the degradation efficiency due to the scavenging effect of excessive H_2O_2 to hydroxyl radical (refer to Equation 2.6 and 2.8 in Table 2.1) and the recombination of $\bullet\text{OH}$ (Equation 2.7 in Table 2.1) which reduce the degradation efficiency.

CHAPTER 3

METHODOLOGY AND WORK PLAN

3.1 Materials and Chemicals

The materials and chemical reagents used for the experiment and their respective specifications are listed in Table 3.1.

Table 3.1: List of Chemicals and Their Specifications

Chemical Reagents	Purity (%)	Supplier	Usage
Aniline	≥ 99.5	Sigma Aldrich, Malaysia	To serve as model pollutant
Multiwalled Carbon Nanotubes (MWCNTs)	> 95	Fisher Scientist, Malaysia	To be used in MMWCNTs synthesis
Fe ₃ O ₄ powder	97	Sigma Aldrich, Malaysia	To be used in MMWCNTs synthesis
Nitric Acid (HNO ₃)	65	Merck, Malaysia	To functionalize pristine MWCNTs
H ₂ O ₂	≥ 30	Sigma Aldrich, Malaysia	To serve as oxidant
Hydrochloric Acid (HCl)	37	Sigma Aldrich, Malaysia	To be used for pH adjustment
Sodium Hydroxide (NaOH)	97	Sigma Aldrich, Malaysia	To be used for pH adjustment
Ethanol	95	Sigma Aldrich, Malaysia	To dissolve aniline

3.2 Equipment

List of equipment and instruments with their function is shown in Table 3.2.

Table 3.2: List of Instruments and Functions

Instrument	Function
pH meter	To measure the pH of solution
Hot plate with magnetic stirring bar	To heat and mix the MWCNTs with nitric acid
Shaking incubator	To mix MMWCNTs, aniline with H ₂ O ₂ and mix MWCNTs with Fe ₃ O ₄
Oven	To dry the synthesized MMWCNTs nanocomposite
Sonicator	To disperse the MWCNTs in Fe ₃ O ₄ solution and disperse the used MMWCNTs in ethanol
Microbalance	To measure of weight of MWCNTs and MMWCNTs
X-Ray Diffractometer	To identify the crystalline phase of sample
Fourier Transform Infrared Spectrometer	To identify the functional group of sample
UV-vis Spectrophotometer	To measure the concentration of aniline
Brunauer–Emmett–Teller	To determine the specific surface area of sample
Thermogravimetric Analysis	To analyse the thermal stability of sample

3.3 Overall Experiment Flowchart

The overall flowchart of this experiment was illustrated in Figure 3.1. First, acid pre-treatment of the pristine MWCNTs was carried out to produce MWCNTs-COOH. Next, the MWCNTs- Fe₃O₄ magnetic nanocomposites were synthesized by applying the direct doping technique. Next, the resultant nanocomposites were characterized by using FTIR, XRD, SEM-EDX, BET and TGA. After that, operating parameter studies were performed based on the 20 sets of experiments generated by Design Expert software. Parameters such as effect of solution pH, Fe₃O₄-MWCNTs dosage, and H₂O₂ dosage were studied. The liquid sample analysis was done using UV-visible spectrophotometer. Optimum condition for

simultaneous adsorption and degradation of aniline via Fenton reagent was determined by Design Expert from the results of the 20 sets experiments.

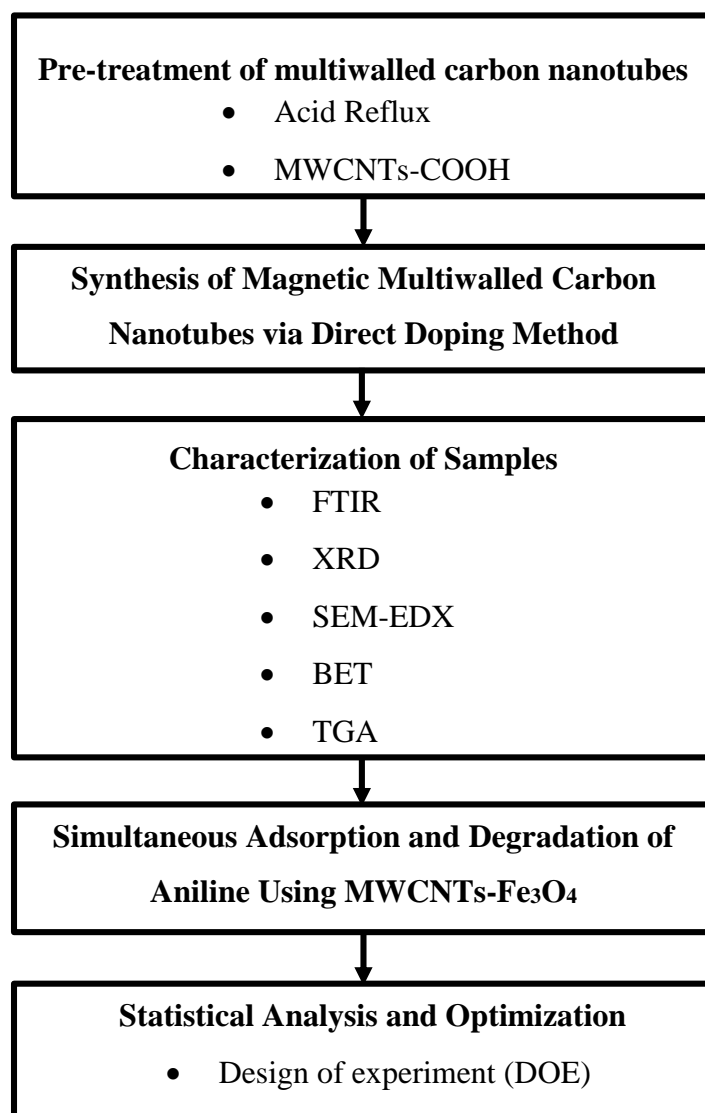


Figure 3.1: Overall Flowchart of Experiment

3.4 Preparation of MWCNTs-Fe₃O₄

The preparation of MWCNTs-Fe₃O₄ via direct doping method involved 2 main steps. The first step was the pre-treatment and functionalization of MWCNTs while the second step was the synthesis of MWCNTs-Fe₃O₄ by direct doping.

3.4.1 Pre-treatment and functionalization of MWCNTs

The purpose of carry out pre-treatment and functionalization of MWCNTs is to remove the impurity from the pristine MWCNTs and to create the functional group of -COOH on MWCNTs. First, 1 g of pristine MWCNTs was poured into the conical flask containing 100 ml of HNO₃. Next, the mixture was mixed ultrasonically for 1 hour, followed by refluxing the mixture for 6 hours at 80 °C. After 6 hours, the treated MWCNTs was filtered and washed with distilled water for a few times. Then, the treated MWCNTs were dried at 80 °C for 24 hours. The functionalized MWCNT, MWCNTs-COOH were obtained.

3.4.2 Direct Doping

To synthesize MWCNTs-Fe₃O₄, the ratio of MWCNTs-COOH to Fe₃O₄ was set to 1.5:1. First, the required amount of MWCNTs-COOH and Fe₃O₄ were ultrasonicated in 15 mL deionized water separately for 30 minutes. Then pH of both dispersions were adjusted to pH 4.5-4.6 by using NaOH and HCl. The predetermined amount of Fe₃O₄ were added into MWCNTs-COOH. Then the mixture was ultrasonicated for 5 minutes for homogeneous dispersion of MWCNTs-COOH and Fe₃O₄. The mixture was then transferred to a conical flask and was rotated 24 hours with the aid of shaking incubator at 200 rpm at room temperature. The well-mixed MWCNTs-Fe₃O₄ were obtained. To separate and filter out the MWCNTs-Fe₃O₄ from the mixture, magnet harvesting was applied for 30 minutes. The harvested MWCNTs-Fe₃O₄ were rinsed with distilled water for several times. Lastly, the MWCNTs-Fe₃O₄ was dried for 24 hours at 80 °C in the oven.

3.5 Characterization of pristine MWCNTs, MWCNTs-COOH and MWCNTs-Fe₃O₄

Characterization of pristine MWCNTs, MWCNTs-COOH and MWCNTs-Fe₃O₄ is important to study the properties of the magnetic nanocomposites synthesized such as the functional group, crystallographic, morphology and elemental analysis. The characterizations of samples were done by using FTIR, XRD, SEM-EDX, BET and TGA.

3.5.1 FTIR

FTIR spectrometer model Nicolet IS10 supplied by Thermo Fisher Scientific was used to identify the functional group presented in the MWCNTs-COOH, and synthesized MWCNTs-Fe₃O₄. FTIR technique was used to ensure that the functionalized MWCNTs embedded with Fe₃O₄ nanoparticles was successfully synthesized by identification of presence of O-H and Fe-O-Fe stretching. A mixture of sample and potassium bromide (KBr) was pelletized into thin film. The IR spectrum was collected after 32 scans.

3.5.2 XRD

X-ray diffractometer model XRD-6000 with Cu-K α radiation at current of 30 mA and voltage of 40 kV supplied by Shimadzu was used to determine the composition of the pristine MWCNTs, functionalized MWCNT-COOH, MWCNTs-Fe₃O₄ and used MWCNTs-Fe₃O₄. Scanning speed of 2 °/min in the angular range, 2 θ from 10 - 80° was set. The sample was first grounded and located into the sample holder. X-rays was focused on the sample and diffracted. Then, the changes in the intensities of X-rays was recorded continuously. The composition was identified based on the peaks obtained.

3.5.3 SEM-EDX

The surface morphology and the composition of elements for pristine MWCNTs, MWCNTs-COOH and MWCNTs-Fe₃O₄ were analysed by using Hitachi SEM model S-3400N. Firstly, the sample was located on the sample holder with aid of double-sided adhesive tape. Before the analysis, the sample was coated with gold and platinum for 135 second to obtain clearer image. Then the beam with 15 kV energy was turned on to start the analysis. The image formed was analysed. Coupling SEM with EDX, identification of elemental composition was done.

3.5.4 BET

The specific surface area of pristine MWCNT, MWCNTs-COOH and MWCNTs-Fe₃O₄ were determined using BET analysis. To determine the specific surface area, the N₂ adsorption desorption isotherm were obtained at

liquid nitrogen temperature (-195.866 °C) using a Micromeritics ASAP 2010M instrument. Then, by using Brunauer–Emmett–Teller (BET) equation, the specific surface areas of samples were calculated.

3.5.5 TGA

TGA was used to study the thermal stability of MWCNT-COOH and MWCNTs-Fe₃O₄ and their weight loss when the samples were being heated from 30 °C to 1000 °C with heating rate of 10 °C per minutes in constant nitrogen atmosphere. 10 mg of sample was weighed and transferred to the crucible and the analysis was started. The thermal stability and weight loss were analysed from the TGA curve obtained.

3.6 Simultaneous Adsorption and Degradation of Aniline using MWCNTs-Fe₃O₄

All the experiments were performed at a fixed aniline initial concentration of 50 ppm and the operating temperature of 25 °C. A predetermined concentration of aniline was added into a small glass bottle. Then, pH of solution was measured and adjusted using pH meter. Next, the required amount of MWCNTs-Fe₃O₄ was weighed and added into the bottle. Then, the mixture was shaken for 15 minutes at the speed of 200 rpm. After that, the predetermined amount of H₂O₂ was added to the bottle to form a 15 ml mixture. Then, the mixture was shaken for 24 hours using shaking incubator. After 24 hours, magnet was deposited at the side of the small bottle for magnetic isolation of used MWCNTs-Fe₃O₄ from the mixture. The concentration of aniline remained in sample was analysed by UV-vis spectrophotometer.

To determine the amount of aniline being adsorbed, the used MWCNTs-Fe₃O₄ were added into 20 ml of ethanol and sonicated for 30 minutes to ensure that the aniline dissolved in ethanol. Magnet harvesting was performed again to separate out the used MWCNTs-Fe₃O₄. Then, the remaining solution sample was analysed with UV-vis spectrophotometer which ethanol was used as blank solution to determine the concentration of aniline adsorbed by MWCNTs-Fe₃O₄.

The removal efficiencies of aniline by simultaneous adsorption and degradation using magnetic multiwalled carbon nanotubes, MWCNTs-Fe₃O₄

were analysed using UV-vis spectrophotometer at the maximum wavelength of 280 nm. The concentration of aniline being adsorbed and degraded were calculated using the following equations:

$$C_{AT} = C_{AO} - C_{A,24} \quad (3.1)$$

$$C_{A,adsorb} = C_{A,ethanol} \quad (3.2)$$

$$C_{A,degrade} = C_{AT} - C_{A,adsorb} \quad (3.3)$$

where

C_{AT} = Total aniline concentration being removed

C_{AO} = Initial concentration of aniline, 50 ppm

$C_{A,24}$ = Aniline concentration after 24 hours

$C_{A,ethanol}$ = Aniline concentration being dissolved in ethanol

$C_{A,adsorb}$ = Aniline concentration being removed by adsorption

$C_{A,degrade}$ = Aniline concentration being removed by degradation

3.7 Statistical Analysis and Optimization Using Design of Experiments (DOE)

The effects of 3 process parameters on the removal efficiency of aniline by adsorption and degradation including solution pH, MWCNTs-Fe₃O₄ dosage and H₂O₂ dosage were studied by utilizing the design of experiments (DOE) using Design Expert Version 11.1.2 (Stat-Ease, Inc.) software. The study type and design type selected for the DOE were response surface method (RSM) and central composite design (CCD) respectively. The coded and actual values of process parameters was shown in Table 3.3 while the design matrix of the experiment was shown in Table 3.4. The relationship between the process parameters with the adsorption and degradation efficiency was analysed by a quadratic model using regression analysis and it was then used to optimize the process.

Table 3.3: Coded and Actual Values of Process Parameters in the Design

Variable	Code	Unit	Level				
			-2 (- α)	-1	0	+1	+2 (+ α)
Solution pH	A	pH	2.00	3.62	6.00	8.38	10.00
MWCNTs-Fe ₃ O ₄ dosage	B	mg	5.00	8.04	12.5	16.96	20.00
H ₂ O ₂ dosage	C	mM	4.00	6.43	10.00	13.57	16.00

Table 3.4: Design Matrix of Experiments with CCD Coded Factors

Run	A: Solution pH (pH)	B: MWCNTs- Fe ₃ O ₄ dosage (mg)	C: H ₂ O ₂ dosage (mM)
1	3.62	8.04	6.43
2	8.38	8.04	6.43
3	3.62	16.96	6.43
4	8.38	16.96	6.43
5	3.62	8.04	13.57
6	8.38	8.04	13.57
7	3.62	16.96	13.57
8	8.38	16.96	13.57
9	2.00	12.50	10.00
10	10.00	12.50	10.00
11	6.00	5.00	10.00
12	6.00	20.00	10.00
13	6.00	12.50	4.00
14	6.00	12.50	16.00
Repeated Experiment			
15	6.00	12.50	10.00
16	6.00	12.50	10.00
17	6.00	12.50	10.00
18	6.00	12.50	10.00
19	6.00	12.50	10.00
20	6.00	12.50	10.00

CHAPTER 4

RESULTS AND DISCUSSION

4.1 Characterization of MWCNTs, MWCNTs-COOH and MWCNTs-Fe₃O₄

4.1.1 FTIR Results

The functional groups of MWCNT-COOH and MWCNTs-Fe₃O₄ synthesized via solvent free direct doping were identified by FTIR analysis and the spectra of samples ranging from 500 to 4000 cm⁻¹ were shown in Figure 4.1. From the MWCNT-COOH spectrum (Figure 4.1 (a)), the peaks at 1630 cm⁻¹ indicated the C=C stretching forming the framework of MWCNT (Nie et al., 2015). Besides, peaks at 2850 cm⁻¹ and 2916 cm⁻¹ were assigned to in-plane bending vibration of C-H stretch vibration, originating from the MWCNTs surface (Fallah-Shojaei et al., 2014). Furthermore, an obvious broad peak ranging from 3500 cm⁻¹ to 3200 cm⁻¹ was observed, attributing to O-H stretching. Moreover, the peak at 1720 cm⁻¹ was attributed to stretching vibration of C-O bonds (Nie et al., 2015). The O-H and C-O peaks observed in MWCNT-COOH spectrum indicated the presence of carboxylic acid group, concluding that the MWCNT was successfully functionalized with nitric acid, forming MWCNT-COOH.

Apart from that, as shown in Figure 4.1 (b), an additional peak at around 600 cm⁻¹ which was found in the spectrum of MWCNTs-Fe₃O₄ indicating the presence of Fe₃O₄. The peak of 600 cm⁻¹ was attributed to the Fe-O-Fe interactions in Fe₃O₄ (Rahmawati et al., 2017), showing that Fe₃O₄ was successfully doped on the surface of MWCNTs to form MWCNTs-Fe₃O₄. Since the peak was not obvious, the presence of Fe₃O₄ was further proven by other characterization methods such as SEM-EDX and XRD.

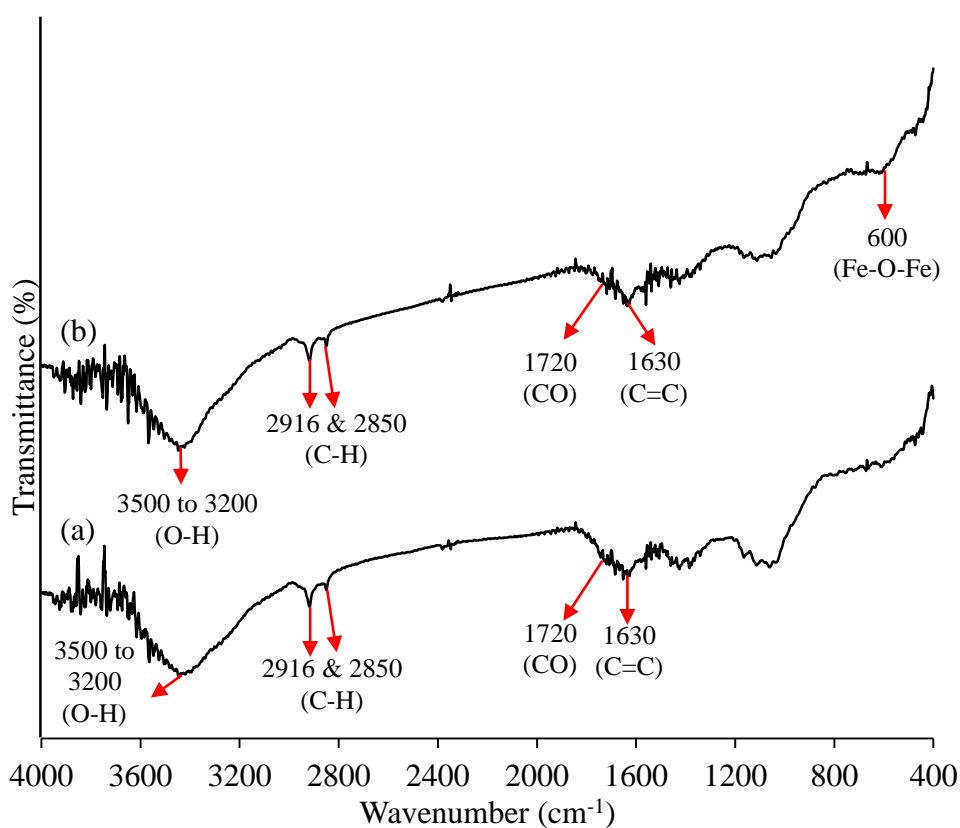


Figure 4.1: FTIR Spectra of (a) MWCNTs-COOH, (b) MWCNTs-Fe₃O₄

4.1.2 XRD Results

The crystal structure of pristine MWCNTs, functionalized MWCNTs (MWCNTs-COOH), synthesised MWCNTs-Fe₃O₄ and used MWCNTs-Fe₃O₄ were analysed using XRD analysis and the XRD patterns obtained were shown in Figure 4.2.

From Figure 4.2 (a) and (b), a broad peak was observed in pristine MWCNTs and MWCNTs-COOH sample respectively at 26.0 ° indicated the hexagonal graphite structure of MWCNTs (Wang et al., 2014). There was no characterization peak of Fe₃O₄ in XRD patterns of MWCNTs and MWCNTs-COOH, indicating that Fe₃O₄ was not doped on the surface of the tubes. Comparing the XRD patterns of pristine MWCNTs and MWCNTs-COOH, both possessed similar XRD patterns, indicating that the acid treatment coupled with ultrasonication did not destroy the hexagonal graphite structure of MWCNTs.

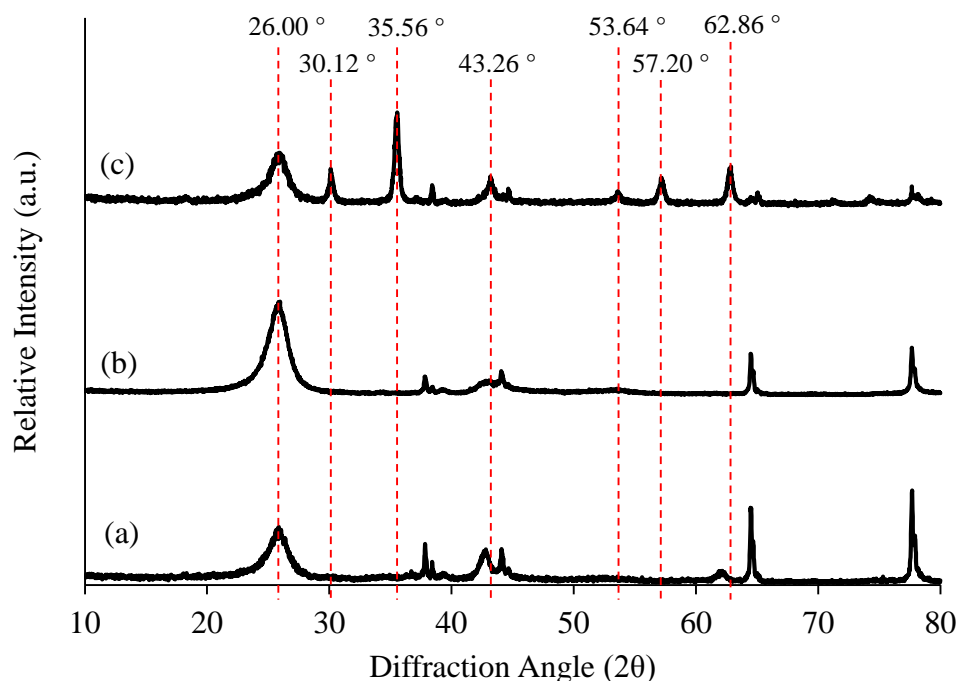


Figure 4.2: XRD Patterns for (a) Pristine MWCNTs, (b) MWCNTs-COOH, (c) Synthesized MWCNTs-Fe₃O₄

From the XRD patterns of MWCNTs-Fe₃O₄ as shown in Figure 4.2 (c), the peaks of hexagonal graphite structure at $2\theta=26.0^\circ$ indicated that the deposition of Fe₃O₄ nanoparticles did not alter the carbon nanotubes' structures. Besides, additional peaks at $2\theta=30.12^\circ$, 35.56° , 43.26° , 53.64° , 57.2° and 62.86° which were tally with the Fe₃O₄ characteristic peaks obtained in literature by Wang et al. (2014) concluded that Fe₃O₄ particles were successfully doped on the surface of MWCNTs, forming MWCNTs-Fe₃O₄.

4.1.3 SEM-EDX results

Figure 4.3 (a), (b) and (c) showed the morphology of pristine MWCNTs, MWCNTs-COOH and MWCNTs-Fe₃O₄ respectively. From Figure 4.3 (a), plenty of MWCNTs bundles could be observed (indicated by the red circle) due to the strong Van der Waals force between them. It can be observed that the pristine MWCNTs possessed smooth surface because no other components presented on the surface of MWCNTs. By observing the morphology of MWCNTs-COOH in Figure 4.3 (b), the bundle shape of MWCNTs could still be observed and the surface was as smooth as pristine MWCNTs (Figure 4.3

(a)), indicating that functionalization of MWCNTs did not destroy the shape of MWCNTs even though MWCNTs were functionalized in harsh condition: ultrasonication for 1 hour in concentrated HNO_3 . From Figure 4.3 (c), it could be observed that the surface of MWCNTs- Fe_3O_4 became rougher as compared to the pristine MWCNTs due to the presence of Fe_3O_4 which is indicated by the red circle. The MWCNTs were linked to each other among the Fe_3O_4 particles. From the morphology, it could be observed that the Fe_3O_4 particles not only embedded on the surface of MWCNTs but some of the particles also agglomerated and formed larger particles which presented as free particles in the composite.

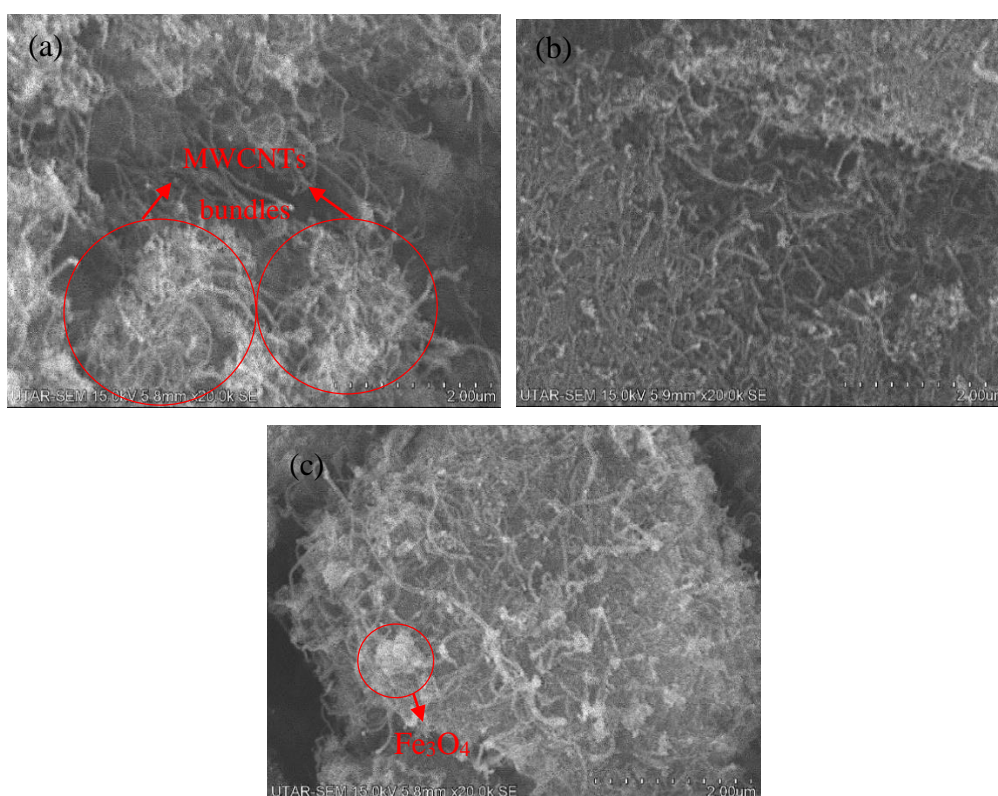


Figure 4.3: SEM Images of (a) Pristine MWCNTs, (b) MWCNTs-COOH, (c) MWCNTs- Fe_3O_4

Furthermore, the elemental composition of pristine MWCNTs, MWCNTs-COOH and MWCNTs- Fe_3O_4 were identified with the aid of EDX and the results obtained were summarized in Table 4.1. MWCNT-COOH had a higher atomic percent of C elements and lower atomic percent of Mg compared to pristine MWCNTs, indicating that the acid pre-treatment successfully

removed impurities from the pristine MWCNTs. Hence, the atomic percent of C element increased after acid pre-treatment. The presence of Fe element in the MWCNTs-Fe₃O₄ samples indicated that Fe₃O₄ was successfully doped onto the MWCNTs surface via solvent free direct doping method.

Table 4.1: Atomic Percent for MWCNTs, MWCNTs-COOH and MMWCNTs

Sample	Atomic Percent (At %)				
	C	O	Mg	Fe	Co
Pristine MWCNTs	72.25	16.60	11.15	-	-
MWCNTs-COOH	97.55	2.27	0.17	-	-
MWCNTs-Fe ₃ O ₄	70.10	13.39	0.23	15.90	0.39

4.1.4 BET Results

BET analysis was used to study the specific surface area of the pristine MWCNTs, MWCNTs-COOH and MWCNTs-Fe₃O₄. BET analysis indicated that MWCNTs-Fe₃O₄ composite poses mesoporous characteristic as the isotherm showed type IV curve and H4 hysteresis loop according to IUPAC (Allothman, 2012).

Table 4.2: BET Results for Samples

	BET surface area (m ² /g)	Pore diameter (nm)	Mesopore volume (cm ³ /g)	Micropore volume (cm ³ /g)	Total pore volume (cm ³ /g)
Pristine MWCNTs	123.78	17.63	0.525	0.025	0.550
MWCNTs-COOH	157.94	33.14	1.293	0.017	1.310
MWCNTs-Fe ₃ O ₄	168.88	29.66	1.238	0.012	1.250

The specific surface areas of pristine MWCNTs, MWCNTs-COOH and MWCNTs-Fe₃O₄ were calculated using BET equation. The specific surface area, pore diameter and pore volume of pristine MWCNTs, MWCNTs-COOH and

MWCNTs-Fe₃O₄ were summarized in Table 4.2. The specific surface area of MWCNTs-Fe₃O₄ was bigger than the pristine MWCNTs and MWCNTs-COOH due to formation of new pores and additional surface on MWCNTs after doping process (Moazzen et al., 2019). The formation of new pores will lead to the increase of active sites for the reactants, hence improved the adsorption and desorption efficiency of aniline.

4.1.5 TGA Results

The thermal stabilities of MWCNTs-COOH and MWCNTs-Fe₃O₄ were studied using TGA. The TGA curves obtained were shown in Figure 4.4 while the derivative weight loss curve of MWCNTs-COOH and MWCNTs-Fe₃O₄ were shown in Figure 4.5 and Figure 4.6 respectively. The final weight loss for MWCNTs-COOH was 83.08 % while the weight loss for MWCNTs-Fe₃O₄ was 72.02 %. The smaller weight loss of MWCNTs-Fe₃O₄ compared to MWCNTs-COOH indicated that the thermal stability of MWCNTs-Fe₃O₄ was higher than MWCNTs-COOH (Sadegh, Shahryari-ghoshekandi and Kazemi, 2014). From MWCNTs-COOH TGA curve in Figure 4.4, a small weight loss observed at lower temperature of 150 °C might due to the removal of water molecules and decomposition of carboxylic and hydroxyl functional group (Huang et al., 2013). Significant weight loss at higher temperature (> 800 °C) can be observed from both MWCNTs-COOH curves and MWCNTs-Fe₃O₄ curves, which was ascribed to the oxidation of carbon nanotubes into carbon dioxide at high temperature (Sadegh, Shahryari-ghoshekandi and Kazemi , 2014).

From the TGA curve of MWCNTs-Fe₃O₄, the smaller weight loss of MWCNTs-Fe₃O₄ compared to MWCNTs-COOH concluded that doping of Fe₃O₄ onto the surface of MWCNTs-Fe₃O₄ enhanced the thermal stability of the sample by reducing the diffusivity of components with lower volatility because the Fe₃O₄ nanoparticles which had a stable thermal stability up to 1000 °C acted as barriers to heat permeability into the catalyst (Kong, Ahmad and Shanks, 2016). The smaller weight loss in MWCNTs-Fe₃O₄ also confirmed the successful doping of Fe₃O₄ onto the MWCNTs.

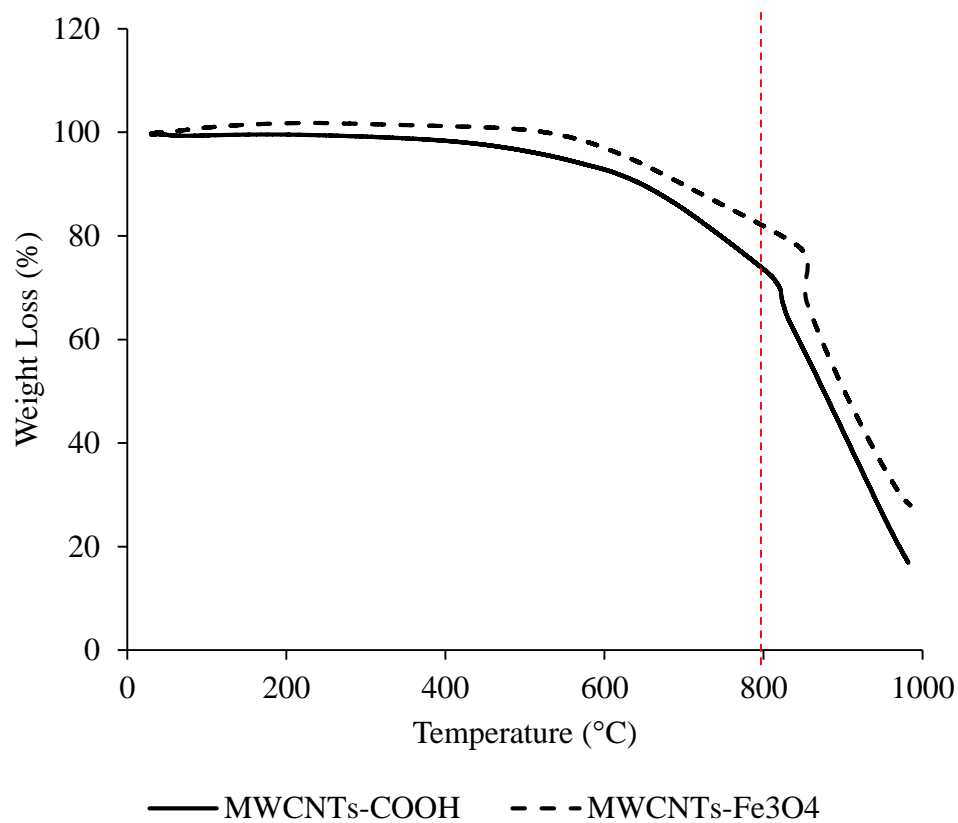
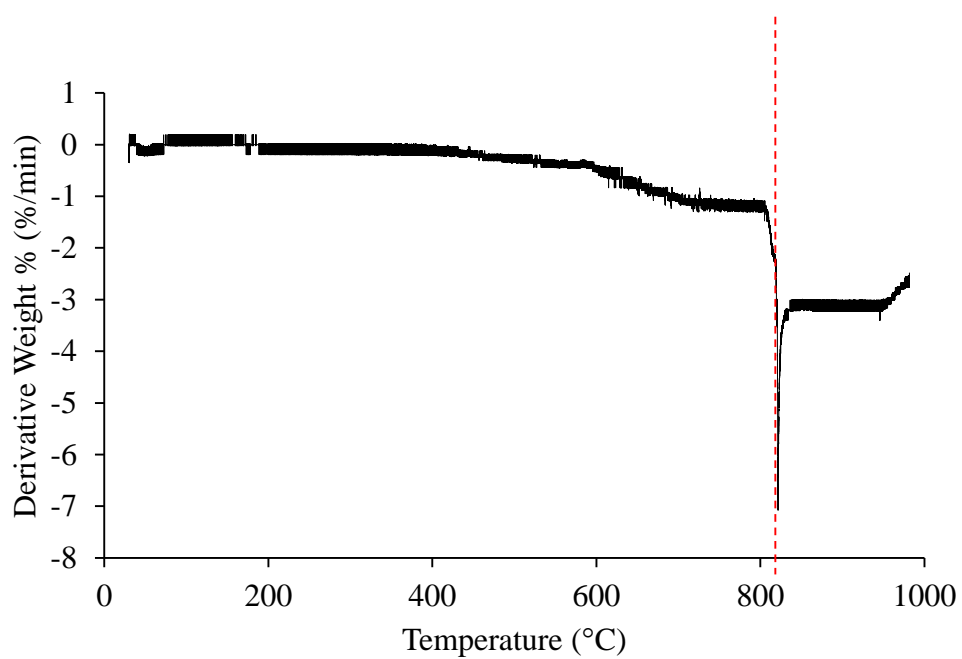
Figure 4.4: TGA Curves for MWCNTs-COOH and MWCNTs-Fe₃O₄

Figure 4.5: Derivative Weight Loss Curve of MWCNTs-COOH

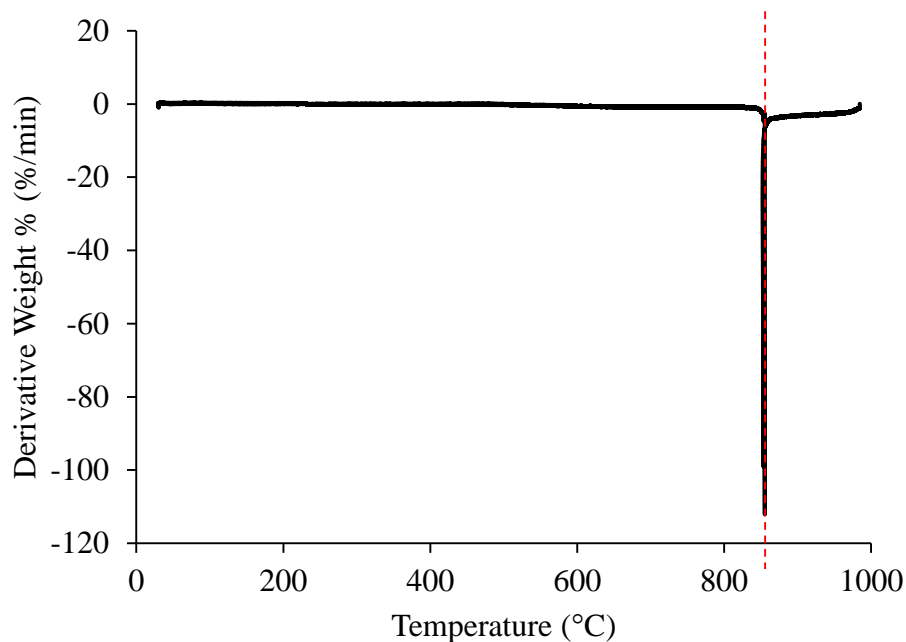


Figure 4.6: Derivative Weight Loss Curve of MWCNTs-Fe₃O₄

4.2 Statistical Analysis and Optimization Study

Response surface methodology (RSM) was used to study the relationship between the studied parameters and the aniline removal efficiency by adsorption and degradation. The regression analysis, response surface analysis and parameters optimization were discussed in the following section.

4.2.1 Regression Analysis

Table 4.3 showed the obtained adsorption and degradation efficiencies of aniline with a combination of 3 different process parameters: solution pH (A), MWCNTs-Fe₃O₄ dosage (B) and H₂O₂ dosage (C). The adsorption efficiency of aniline was found in the range of 0 to 29.01% while the degradation of aniline ranged from 0 to 79.37%.

Table 4.3: Experiment Design Conditions and Their Respective Adsorption and Degradation Efficiency

Run	A: Solution pH (pH)	B: MWCNTs- Fe₃O₄ dosage (mg)	C: H₂O₂ dosage (mM)	Adsorption Efficiency (%)	Degradation Efficiency (%)
1	3.62	8.04	6.43	14.44	65.17
2	8.38	8.04	6.43	10.37	8.75
3	3.62	16.96	6.43	15.16	73.84
4	8.38	16.96	6.43	13.96	31.77
5	3.62	8.04	13.57	9.42	67.03
6	8.38	8.04	13.57	10.33	3.31
7	3.62	16.96	13.57	10.39	73.20
8	8.38	16.96	13.57	20.86	21.17
9	2.00	12.50	10.00	6.10	79.37
10	10.00	12.50	10.00	8.08	3.89
11	6.00	5.00	10.00	0.00	0.00
12	6.00	20.00	10.00	20.32	51.28
13	6.00	12.50	4.00	17.37	31.19
14	6.00	12.50	16.00	21.69	27.90
Repeated Experiment					
15	6.00	12.50	10.00	23.81	36.37
16	6.00	12.50	10.00	23.16	25.24
17	6.00	12.50	10.00	26.41	21.95
18	6.00	12.50	10.00	22.09	29.51
19	6.00	12.50	10.00	29.01	18.88
20	6.00	12.50	10.00	23.28	19.70

Then the analysis of variance (ANOVA) on the results obtained was performed. Table 4.4 showed the ANOVA results for adsorption of aniline.

Table 4.4: ANOVA result for Response Surface Model for Adsorption Efficiency of Aniline

Source	Sum of Squares	df	Mean Square	F value	p-value
Model	1006.06	9	111.78	10.06	0.0006
A- Solution pH	6.51	1	6.51	0.5857	0.4618
B- MWCNTs-Fe ₃ O ₄ dosage	183.01	1	183.01	16.47	0.0023*
C- H ₂ O ₂ dosage	1.38	1	1.38	0.1241	0.7320
AB	19.32	1	19.32	1.74	0.2167
AC	34.69	1	34.69	3.12	0.1077
BC	6.48	1	6.48	0.5831	0.4627
A ²	495.08	1	495.08	44.55	< 0.0001*
B ²	328.59	1	328.59	29.57	0.0003*
C ²	30.81	1	30.81	2.77	0.1268
Residual	111.13	10	11.11		
Lack of Fit	77.66	5	15.53	2.32	0.1885
Pure Error	33.47	5	6.69		
Cor Total	1117.19	19			

R²=0.9005; Adjusted R²=0.8110; Standard Deviation=3.33; Mean=16.31

* Significant at 95% confident level

From Table 4.4, the value of determination coefficient, R² for the adsorption model was found to be 0.9005, which was higher than 0.90. This indicated that the quadratic regression model fitted the data well. Most of the variation of the efficiency could be explained by the different parameter values. The significance of the regression model could be further explained by the model F-value and p-value. For the adsorption regression model, the F-value is 10.06 with a p-value of 0.0006, implying the model was significant as only a chance of 0.06 % that an F-value this large could happen because of noise. The validity of model could be further proved by the insignificant lack of fit. The lack of fit value of 2.32 indicated that the lack of fit was not significant

compared to pure error, showing that the model fitted the data well. Besides, it could be observed from Figure 4.7 that most of the actual experimental values point were close to the predicted values trend line, indicating the experimental values fitted the predicted values well. In short, the developed quadratic regression model successfully correlated the adsorption efficiency of aniline using MWCNTs-Fe₃O₄ to different process parameters.

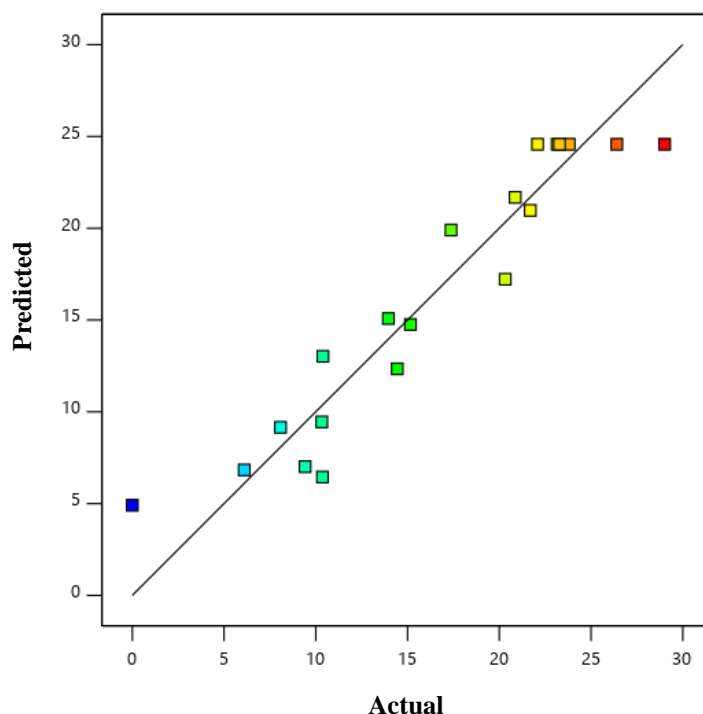


Figure 4.7: Actual and Predicted Values of Adsorption Efficiency of Aniline ($R^2=0.9005$)

The model term is significant to the model if it has a p-value smaller than 0.05. From Table 4.4, terms B, A² and B² had p-value smaller than 0.05. Hence, the significant terms of the model included B, A² and B², indicating both pH and MWCNTs-Fe₃O₄ dosage had significant impact on adsorption of aniline. Values larger than 0.1 indicated that the model terms are not significant. High p-value of term C indicated that H₂O₂ dosage was not a significant process parameter in aniline adsorption. Besides, the interaction between the 2 parameters (A and B) was not that significant in affecting the adsorption efficiency which could be explained by the term AB p-value which was larger than 0.10. Equation 4.1 showed the quadratic model equation in coded factor

which related the aniline adsorption efficiency to different parameters after eliminating the insignificant terms.

$$\text{Adsorption Efficiency (\%)} = 24.57 + 0.6903A + 3.66B - 5.86A^2 - 4.78B^2 \quad (4.1)$$

For the response surface model for degradation of aniline using MWCNTs-Fe₃O₄, the ANOVA result was summarized in Table 4.5.

Table 4.5: ANOVA result for Response Surface Model for Degradation Efficiency of Aniline

Source	Sum of Squares	df	Mean Square	F value	p-value
Model	11219.39	9	1246.60	14.53	0.0001
A- solution pH	8524.33	1	8524.33	99.34	< 0.0001*
B- MWCNTs-Fe ₃ O ₄ dosage	1475.96	1	1475.96	17.20	0.0020*
C- H ₂ O ₂ Dosage	30.28	1	30.28	0.3529	0.5657
AB	84.70	1	84.70	0.9870	0.3439
AC	37.26	1	37.26	0.4343	0.5248
BC	7.35	1	7.35	0.0856	0.7758
A ²	913.89	1	913.89	10.65	0.0085*
B ²	76.95	1	76.95	0.8968	0.3660
C ²	196.29	1	196.29	2.29	0.1614
Residual	858.08	10	85.81		
Lack of Fit	633.93	5	126.79	2.83	0.1392
Pure Error	224.14	5	44.83		
Cor Total	12077.46	19			

R²=0.9290; Adjusted R²=0.8650; Standard Deviation=9.26; Mean=34.48

* Significant at 95% confident level

Similar to adsorption regression model, the significance of degradation regression model was studied through the ANOVA study. From ANOVA results in Table 4.5, R^2 for the degradation model was 0.9290. The model F-value was 14.53 with p-value of 0.0001, implying the model was significant. Besides, it had the lack of fit value of 2.83 with p-value of 0.1392 (>0.1), indicating that the lack of fit was not significant relative to pure error. The close relationship between the predicted and actual experimental value as shown in Figure 4.8 further proved the good agreement of experimental value with the predicted model. Hence, it could be concluded that the degradation regression model fitted the experimental data well.

From Table 4.5, it could be found that term A, B and A^2 had p-value less than 0.05, showing that pH and MWCNTs- Fe_3O_4 dosage had significant impacts on degradation of aniline. Term C possessed p-value of larger than 0.05 indicating H_2O_2 dosage did not contribute large impact on the degradation efficiency. This could further be proven by the much smaller coefficient of term C compared to term A and B in quadratic model equation 4.2. From ANOVA, the larger p-value of AB, AC and BC indicated that there was no significant interaction between parameters in affecting the degradation of aniline. Equation 4.2 showed the quadratic model equation in coded factor that illustrated the relationship between different process parameters and aniline degradation efficiency after eliminating the insignificant terms.

$$\begin{aligned} \text{Degradation Efficiency (\%)} = & 24.94 - 24.98A + 10.40B - 1.49C \\ & + 7.96A^2 \end{aligned} \quad (4.2)$$

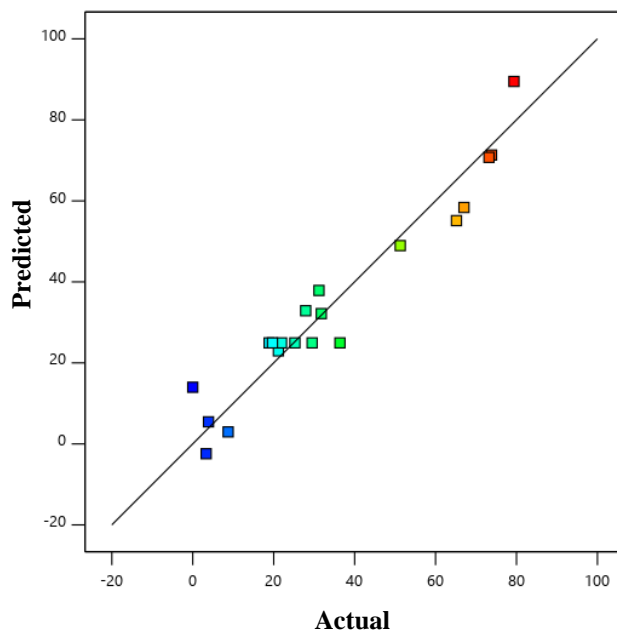


Figure 4.8: Actual and Predicted Values of Degradation Efficiency of Aniline ($R^2=0.9290$)

4.3 Response Surface (RSM) analysis

According to ANOVA results, the adsorption of aniline by MWCNTs-Fe₃O₄ could be affected by several significant parameters such as solution pH (A) and MWCNTs-Fe₃O₄ dosage (B) and their corresponding higher order terms (A² and B²). The higher F-value of the term indicates that the process parameter had a greater impact on the adsorption efficiency. According to Table 4.4, the parameter that had the greatest impact to the adsorption efficiency included higher order of solution pH (A²), followed by higher order of MWCNTs-Fe₃O₄ dosage (B²) and MWCNTs-Fe₃O₄ dosage (B). For degradation of aniline, the parameters which had the significant impacts on degradation efficiency were solution pH (A), MWCNTs-Fe₃O₄ dosage (B), and higher order of solution pH (A²). It was interesting to note that the H₂O₂ dosage was not significant in both adsorption and degradation of aniline.

4.3.1 Effect of solution pH on Adsorption Efficiency of Aniline

Figure 4.9 showed the effects of solution pH on the adsorption efficiency of aniline using MWCNTs-Fe₃O₄. From Figure 4.9, the adsorption efficiency increased when the pH increased from pH 2 to pH 6. However, further increase

of pH from 6 to 10 reduced the adsorption efficiency. The result obtained in this study was consistent with those reported in the literature. Solution pH has great impact on the aniline adsorption efficiency because it alters the ionizability of the aniline, thus causing impact on the interaction of aniline with the adsorbents. Aniline is a weak base which can be protonated to form anilinium ion (protonated aniline molecules) in low pH where the pH is lower than the pKa value of aniline. The pKa value of aniline is reported to be 4.6, meaning that at pH lower than 4.6, aniline exists in the form of acid conjugate (protonated aniline) (Al-Johani and Salam, 2011). Therefore, when the adsorption was performed in the pH less than 4.6, the positively charged aniline will compete with ion H^+ for the available active site on MWCNTs- Fe_3O_4 and thus reducing the adsorption efficiency. Apart from that, the point of zero charge (pH_{pzc}) for MWCNTs- Fe_3O_4 nanocomposites was reported to be 3.8 (Li et al., 2015). At low pH, the surface of MWCNTs- Fe_3O_4 was also positively charged. Therefore, electrostatic repulsion between the protonated aniline and the positively charged MWCNTs- Fe_3O_4 occurred, leading to the decreased of adsorption efficiency.

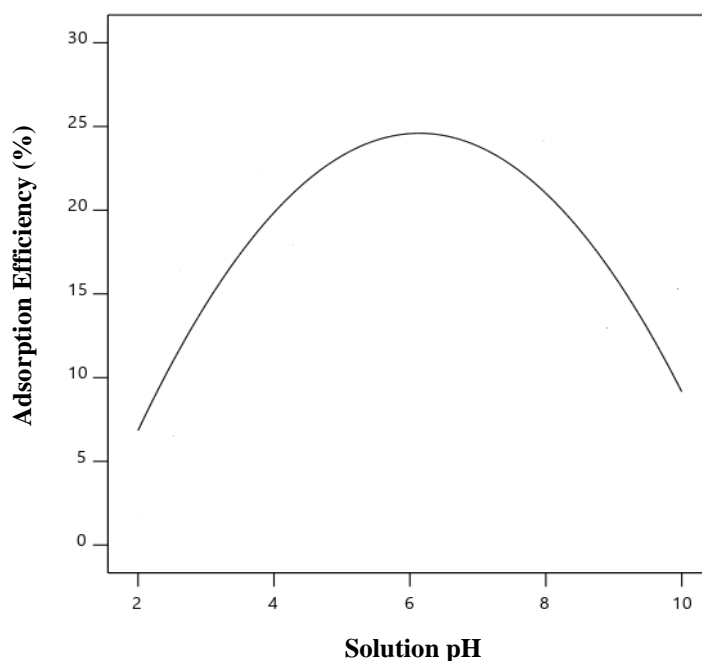


Figure 4.9: Effect of solution pH on Adsorption Efficiency of Aniline by MWCNTs- Fe_3O_4 (MWCNTs- Fe_3O_4 dosage= 12.5 mg, H_2O_2 dosage=10 mM)

Highest adsorption of aniline occurred at pH 6. At this pH, aniline behaves as a neutral molecule and the surface of MWCNTs-Fe₃O₄ became less positive. This reduced the electrostatic repulsion between the MWCNTs-Fe₃O₄ and the protonated aniline molecules. Hence, the adsorption efficiency exhibited a corresponding increase. Further increased the pH from pH 6 to pH 10 significantly reduced the adsorption efficiency. In the base condition, both MWCNTs-Fe₃O₄ surface and aniline became negatively charged. Thus the electrostatic repulsion again caused the decrease of the adsorption efficiency.

4.3.2 Effect of Solution pH on Degradation Efficiency of Aniline

According to studies by Liu et al. (2016) and Wang et al. (2014), heterogeneous Fenton-like reaction can be performed in a wide range of pH due to the enhancement in cycling of Fe²⁺ and Fe³⁺. From Figure 4.10, the highest degradation of aniline occurred at pH 2. It could be observed that the degradation of aniline occurred at wide range of pH but the efficiency decreased with the increase of solution pH. At low pH, stable oxonium ion (H₃O₂⁺) was formed from the H₂O₂, improving the scavenging effect of the hydroxyl radicals (•OH). Hydroxyl radicals exhibited a greater oxidation capacity under acidic conditions. Hence, the decomposition of H₂O₂ into H₂O and O₂ was inhibited (Zhou et al., 2014). At high pH, the decomposition of H₂O₂ to H₂O and O₂ under alkaline conditions was favoured, thereby reducing the concentration of H₂O₂ for Fenton reaction. The decrease in H₂O₂ concentration reduced the generation of •OH radicals for the degradation. Thus, the degradation efficiency of aniline decreased with increasing pH (Bento et al., 2019).

Besides, the stability of H₂O₂ in different pH might cause this trend. According to Jung et al. (2009), H₂O₂ was more stable in lower pH. At low pH, the H₂O₂ decomposition rate was constant within a long period. However, for an unbuffered solution, H₂O₂ decomposition rate was high at the beginning but the rate decreases after a period of time. From Figure 4.10, the lower efficiency at higher pH could occur due to the unstable decomposition of H₂O₂ within the 24-hours period.

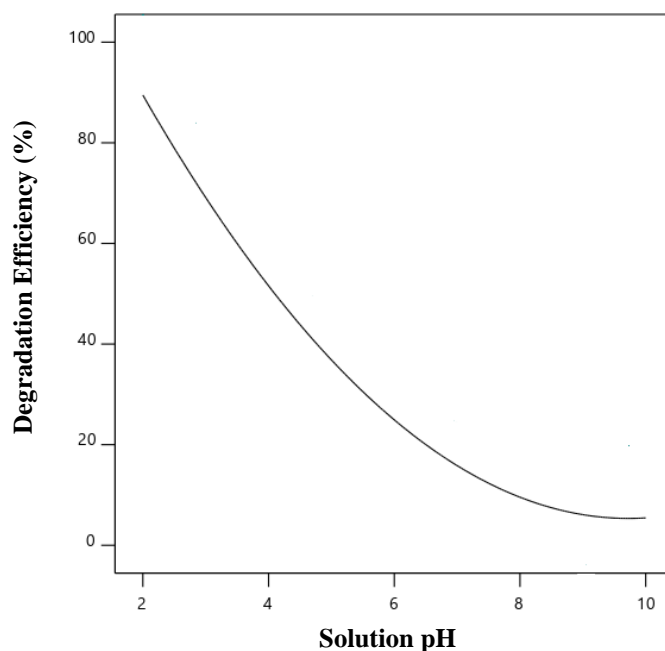


Figure 4.10: Effect of Solution pH on Degradation Efficiency of Aniline by MWCNTs-Fe₃O₄ (MWCNTs-Fe₃O₄ dosage= 12.5 mg, H₂O₂ dosage=10 mM)

4.3.3 Effect of MWCNTs-Fe₃O₄ dosage on Adsorption Efficiency of Aniline

According to Figure 4.11, the adsorption efficiency increased when the MWCNTs-Fe₃O₄ dosage increased from 5 mg to 12.56 mg. This might be because the increase of MWCNTs-Fe₃O₄ dosage would increase the surface area of adsorbent. Besides, higher MWCNTs-Fe₃O₄ dosage increased the available adsorption site for aniline adsorption (Abdel Salam, Gabal and Obaid, 2012). Therefore, more aniline molecules can be adsorbed onto MWCNTs-Fe₃O₄. As shown in Figure 4.11, highest adsorption occurred at MWCNTs-dosage of 12.56 mg. Further increase of adsorbent dosage from 12.56 mg to 20 mg caused the decrease of the adsorption of aniline. At high dosage of MWCNTs-Fe₃O₄, the distance between the MWCNTs-Fe₃O₄, the distance between the MWCNTs-Fe₃O₄ will be reduced and nanocomposites of MWCNTs-Fe₃O₄ will stay close to each other, causing the overlapping of the adsorption sites. Eventually, the total surface area available for adsorption was reduced (Ndi Nsami and Ketcha Mbadcam, 2013).

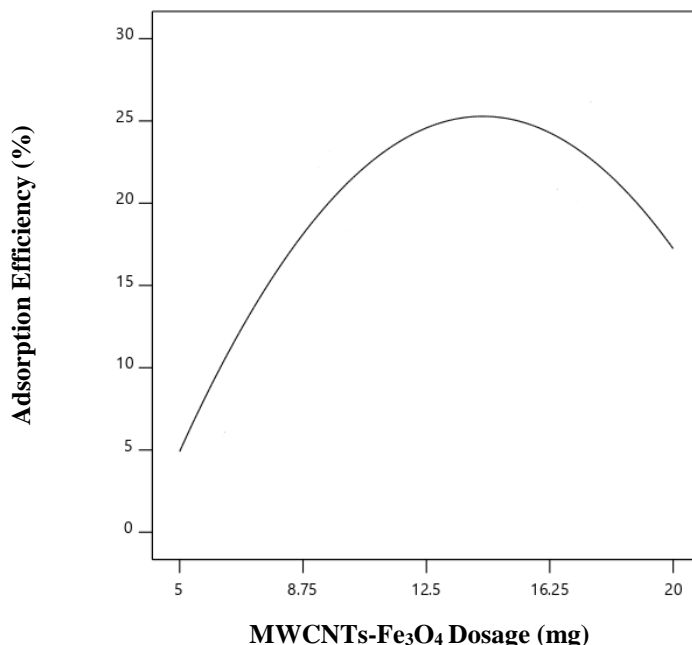


Figure 4.11: Effects of MWCNTs-Fe₃O₄ dosage on Adsorption Efficiency of Aniline by MWCNTs-Fe₃O₄ (Solution pH: pH 6, H₂O₂ dosage=10 mM)

4.3.4 Effect of MWCNTs-Fe₃O₄ dosage on Degradation Efficiency of Aniline

The effect of MWCNTs-Fe₃O₄ dosage in the degradation of aniline exhibited a different result trend as compared to the effect of MWCNTs-Fe₃O₄ in the adsorption of aniline. From Figure 4.12, it could be observed that increasing the MWCNTs-Fe₃O₄ dosage from 5mg to 20 mg increased the degradation efficiency and the highest degradation of aniline occurred at 20 mg of MWCNTs-Fe₃O₄. In the degradation of aniline, MWCNTs-Fe₃O₄ were used as the catalyst to produce hydroxyl radicals from H₂O₂ which were used to degrade pollutant into carbon dioxide and water (Wang et al., 2013). An increase in MWCNTs-Fe₃O₄ dosage provided more iron sites on the surface of catalyst. Thus, more active sites were available and thus accelerated the decomposition of H₂O₂ and dissolution of iron to form more free radicals to degrade the aniline (Zhou et al., 2014). Hence, the efficiency of aniline degradation increased.

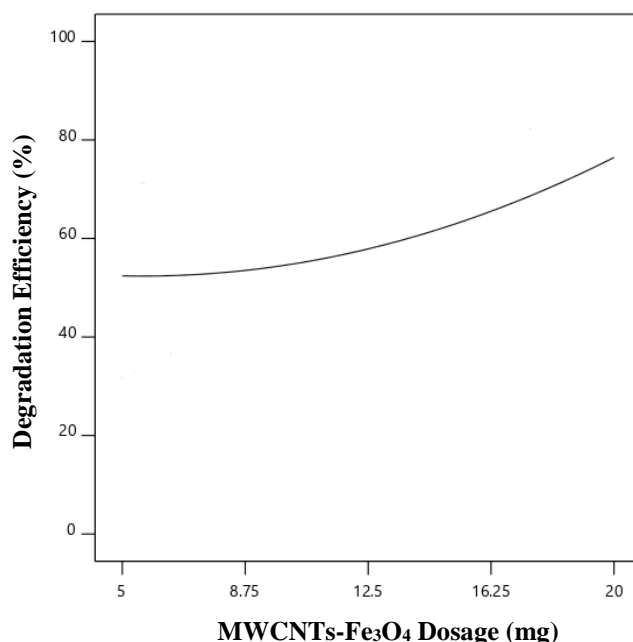


Figure 4.12: Effects of MWCNTs-Fe₃O₄ dosage on Degradation Efficiency of Aniline by MWCNTs-Fe₃O₄ (Solution pH: pH 3.62, H₂O₂ dosage=10 mM)

4.3.5 Effect of H₂O₂ dosage on Degradation Efficiency of Aniline

Since the adsorption of aniline did not involve H₂O₂, therefore H₂O₂ dosage is not significant for adsorption efficiency. However, H₂O₂ played a fundamental role in the Fenton degradation of aniline. Hence, the effect of H₂O₂ dosage on the degradation efficiency of aniline was discussed in this section.

As shown in Figure 4.13, it could be observed that the change of degradation efficiency was not significant with the increment of H₂O₂ dosage from 6.43 mM to 13.57 mM. This observation was further supported by ANOVA analysis shown in Table 4.5 in which H₂O₂ dosage was not a significant parameter compared to solution pH and MWCNTs-Fe₃O₄ dosage. From Figure 4.13, the degradation efficiency only varied from around 55 % to 60 % with increasing H₂O₂ dosage from 6.43 mM to 13.57 mM. However, according to studies by Zhou et al. (2014) and Jia et al. (2019), the removal efficiency had a great improvement when the H₂O₂ dosage increased due to the increased generation of •OH radicals to help in the oxidative degradation. However, it was reported also further increase of dosage did not improve the degradation efficiency due to the scavenging effect where the excess of H₂O₂ scavenged the produced hydroxyl radicals in the solution (Equation 4.3 and 4.4),

making them unavailable for degradation. Besides, the recombination of hydroxyl radicals with each other (Equation 4.5) also reduced the degradation efficiency (Zhou et al., 2014).



The insignificant effect of H_2O_2 dosage in this study indicated that 6.43 mM of H_2O_2 was actually sufficient to produce hydroxyl radical for the degradation of aniline. Hence, this could be the advantage in the degradation process for aniline as the consumption of corrosive chemical (H_2O_2) was low. Similar findings were reported by Liu et al. (2016) which showed that the degradation efficiency of more than 90 % could be achieved using only 5 mM of H_2O_2 dosage with the aid of Ni-Fe oxalate catalyst. This further proved that low dosage of H_2O_2 was sufficient for the aniline degradation. No reduction of efficiency was observed at higher dosage of H_2O_2 indicated that scavenging effect did not occur at this range of H_2O_2 dosage.

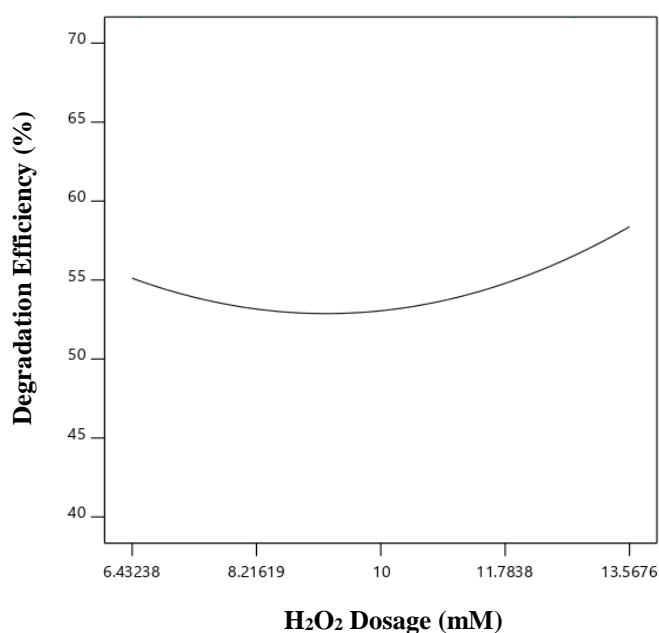


Figure 4.13: Effects of H_2O_2 dosage on Degradation Efficiency of Aniline by MWCNTs- Fe_3O_4 (Solution pH: pH 3.62, MWCNTs- Fe_3O_4 dosage=8.04 mg)

4.3.6 Optimization of Process Parameter

To optimize the adsorption and degradation efficiency of aniline, optimization function embedded in Design Expert software was utilized after the regression model was formed. The constraints used to optimize the process were summarized in Table 4.6. The solution generated from numerical optimization as well as the predicted and experimental result were shown in Table 4.7. The experimental result was obtained by taking the average result of 5 repeated experimental runs conducted based on the optimum solution suggested by Design Expert. From Table 4.7, it could be observed that the difference between predicted and actual optimum efficiency for both adsorption and degradation was very small (< 5%), indicating that the developed model was valid to predict the response factor for real conditions. In conclusion, the optimum adsorption and degradation efficiency of 21.21 % and 56.91 % respectively were obtained when solution of pH 3.71, MWCNTs-Fe₃O₄ dosage of 14.48 mg and H₂O₂ dosage of 6.43 mM were used.

Table 4.6: Constraints for Optimization of Aniline Adsorption and Degradation Efficiencies

Variable	Goal	Lower Limit	Upper Limit
A: Solution pH (pH)	In range	3.62	8.38
B: MWCNTs-Fe ₃ O ₄ dosage (mg)	In range	8.04	16.96
C: H ₂ O ₂ Dosage (mM)	In range	6.43	13.57
Adsorption Efficiency (%)	Maximize	0.00	29.01
Degradation Efficiency (%)	Maximize	0.00	79.37

Table 4.7: Model Validation Conducted at Optimum Condition Generated by Design Expert

Variable	Value
A: Solution pH (pH)	3.71
B: MWCNTs-Fe ₃ O ₄ dosage (mg)	14.48
C: H ₂ O ₂ Dosage (mM)	6.43
Predicted Adsorption Efficiency (%)	18.32
Actual Adsorption Efficiency (%)	21.21
Predicted Degradation Efficiency (%)	63.59
Actual Degradation Efficiency (%)	59.61
Difference in Adsorption Efficiency (%)	2.89
Difference in Degradation Efficiency (%)	3.98

4.4 Effects of Simultaneous Adsorption and Degradation of Aniline on the Structure of MWCNTs-Fe₃O₄

The used MWCNTs-Fe₃O₄ were collected and analysed using XRD after the simultaneous adsorption and degradation process. The XRD patterns of produced MWCNTs-Fe₃O₄ and used MWCNTs-Fe₃O₄ were illustrated in Figure 4.14.

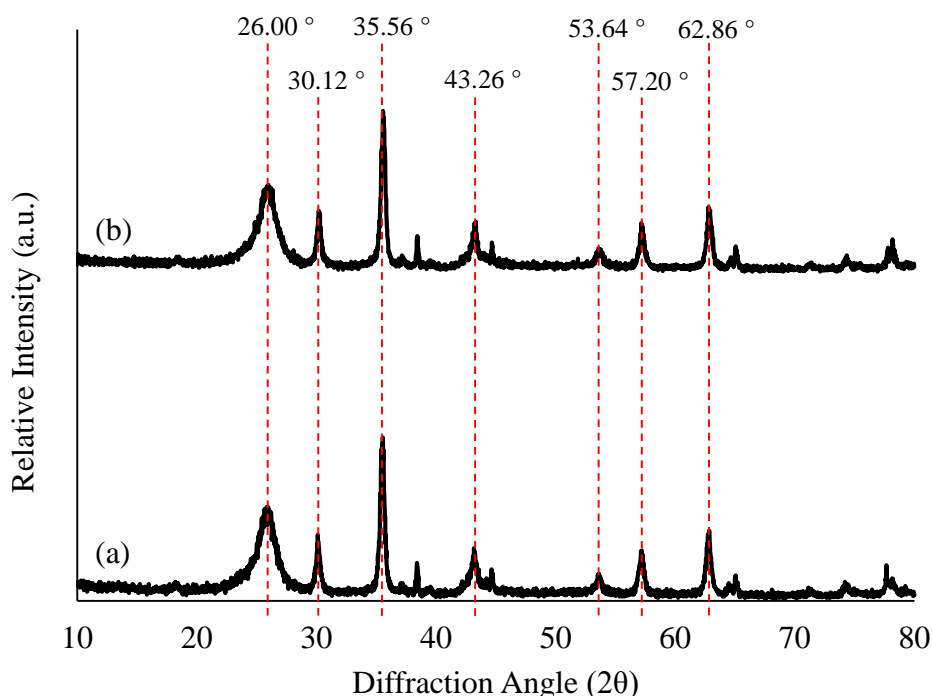


Figure 4.14: XRD Patterns for (a) Synthesized MWCNTs-Fe₃O₄ (b) Used MWCNTs- Fe₃O₄

The similar patterns of both newly produced and used MWCNTs-Fe₃O₄ explained that the adsorption and degradation process did not damage the MWCNTs-Fe₃O₄ structure and MWCNTs-Fe₃O₄ could be recycle for aniline adsorption and degradation to prevent wasting of catalyst.

CHAPTER 5

CONCLUSIONS AND RECOMMENDATIONS

5.1 Conclusions

In this study, magnetic multiwalled carbon nanotubes, MWCNTs-Fe₃O₄ were successfully synthesised in 2 main steps: pre-treatment of MWCNTs by acid reflux followed by solvent free direct doping method. Then, characterizations of the synthesised MWCNTs-Fe₃O₄ were done by FTIR, XRD, SEM-EDX, BET and TGA. Fe₃O₄ peaks were observed in MWCNTs-Fe₃O₄ XRD patterns but not in other samples indicated that the doping of Fe₃O₄ was successful. On the other hand, FTIR analysis also indicated the presence of several functional group in MWCNTs-Fe₃O₄, which were C=C, C-H, O-H, C-O and Fe-O-Fe. SEM image depicted that Fe₃O₄ particles were deposited on the wall of MWCNTs bundles as well as presented as free particles in the composites. The Fe element which could be traced from EDX analysis further confirmed the successful doping of Fe₃O₄ on the MWCNTs. Furthermore, TGA analysis concluded that MWCNTs-Fe₃O₄ possessed smaller weight loss compared to MWCNTs-COOH, indicating higher thermal stability as compared to MWCNTs-COOH. In addition, BET analysis showed that the surface area of MWCNTs-Fe₃O₄ was higher than MWCNTs and MWCNTs-COOH, hence enhancing the active sites for adsorption and degradation of aniline.

The effects of different process parameters on adsorption and degradation efficiencies of aniline and optimization of process parameter were performed with the aid of Design Expert software using RSM with CCD model. The parameters studied included solution pH (pH 2-10), MWCNTs-Fe₃O₄ dosage (5-20 mg) and H₂O₂ dosage (4-16 mM). From the study, it could be concluded that the optimum pH for adsorption occurred at pH 6 while lower pH (pH 2-3) was suitable for degradation. On the other hand, the efficiency for both adsorption and degradation increased with increasing of MWCNTs-Fe₃O₄ dosage. Apart from that, efficiency of adsorption was not affected by H₂O₂ dosage while degradation efficiency was not significantly affected by increasing H₂O₂ dosage. A total optimum removal percentage predicted by Design Expert

was 81.91%: 18.32 % of removal by adsorption and 63.59% of removal by degradation. The actual total optimum removal percentage obtained was 80.82%: 21.21% of removal by adsorption while 59.61% by degradation, revealing the validity of the predicted model.

5.2 Recommendations for Future Work

Other than solution pH, MWCNTs-Fe₃O₄ dosage and H₂O₂ dosage, the initial aniline concentration and temperature should also be considered in the process parameters study. Different initial aniline concentration and temperature may have different effects to both adsorption and degradation efficiency. Besides, accuracy of liquid sample analysis may be affected by the presence of intermediate products with benzene ring. In this study, aniline concentration was measured using UV-visible spectroscopy at 280 nm which was associated with the benzene rings. The aniline might degrade into the intermediate products which consists of benzene ring before it turned into carbon dioxide and water, leading less accuracy in determining the aniline concentration (Liu et al., 2016). To improve the accuracy, gas chromatograph supplied with a flame ionization detector and a column can be used to identify the aniline. The ion chromatograph can be used for intermediates analysis (Huang et al., 2012).

REFERENCES

- Abdel Salam, M., Gabal, M.A. and Obaid, A.Y., 2012. Preparation and characterization of magnetic multi-walled carbon nanotubes/ferrite nanocomposite and its application for the removal of aniline from aqueous solution. *Synthetic Metals*, 161(23–24), pp.2651–2658.
- Adeleke, O.A., Latiff, A.A.A., Saphira, M.R., Daud, Z., Ismail, N., Ahsan, A., Ab Aziz, N.A., Al-Gheethi, A., Kumar, V., Fadilat, A. and Apandi, N., 2019. Principles and Mechanism of Adsorption for the Effective Treatment of Palm Oil Mill Effluent for Water Reuse. *Nanotechnology in Water and Wastewater Treatment*, pp.1–33.
- Al-Johani, H. and Salam, M.A., 2011. Kinetics and thermodynamic study of aniline adsorption by multi-walled carbon nanotubes from aqueous solution. *Journal of Colloid and Interface Science*, 360(2), pp.760–767.
- Alothman, Z.A., 2012. A review: Fundamental aspects of silicate mesoporous materials. *Materials*, 5(12), pp.2874–2902.
- Alsharif, J.M.A., Taha, M.R. and Khan, T.A., 2017. Physical Dispersion of Nanocarbons In Composites–A Review. *Jurnal Teknologi*, 79(5).
- Amritha, A.S. and Manu, B., 2016. FENTON AND PHOTO FENTON OXIDATION OF 2-NITROANILINE. *IJRET: International Journal of Research in Engineering and Technology*, 05(18), pp.2321–7308.
- Anotai, J., Lu, M.-C. and Chewpreecha, P., 2006. Kinetics of aniline degradation by Fenton and electro-Fenton processes. *Water Research*, 40(9), pp.1841–1847.
- Baneshi, M.M., Zarei, A., Ebrahimzadeh, G., Narooie, M.R., Mehrizi, E.A., Mobini, M., Karimi, A. and Biglari, H., 2017. Aniline bio-Adsorption from aqueous solutions using dried activated sludge. *Pollution Research*, 36(3), pp.403–409.
- Bento, A.C., Emídio, E.S., Hammer, P. and Nogueira, R.F.P., 2019. Degradation of acid red 8 dye using photo-fenton reaction mediated by titanium modified catalysts. *Journal of the Brazilian Chemical Society*, 30(10), pp.2170–2181.
- Bottom, R., 2008. Thermogravimetric Analysis. *Principles and Applications of Thermal Analysis*, pp.87–118.
- Cheng, J.P., Zhang, X.B., Yi, G.F., Ye, Y. and Xia, M.S., 2008. Preparation and

magnetic properties of iron oxide and carbide nanoparticles in carbon nanotube matrix. *Journal of Alloys and Compounds*, 455(1–2), pp.5–9.

Costa, S., Borowiak-Palen, E., Kruszyńska, M., Bachmatiuk, A. and Kaleńczuk, R.J., 2008. Characterization of carbon nanotubes by Raman spectroscopy. *Materials Science-Poland*, 26(2).

Department of Natural Resources & Environment - State of Michigan, 2010. *Training Manual for Operators of Wastewater Stabilization Lagoons*. [online] Available at: <https://www.michigan.gov/documents/deq/wrd-ot-lagoon-manual_426356_7.pdf> [Accessed 20 Jul. 2019].

Dutrow, B.L. and Clark, C.M., 2019. *X-ray Powder Diffraction (XRD)*. [online] Available at: <https://serc.carleton.edu/research_education/geochemsheets/techniques/XRD.html> [Accessed 3 Aug. 2019].

EPA, 2016. *Aniline*. [online] Available at: <<https://www.epa.gov/sites/production/files/2016-08/documents/aniline.pdf>> [Accessed 26 Jun. 2019].

Eskander, S. and Saleh, H.E.M., 2017. Biodegradation : Process Mechanism. *Biodegradation and Bioremediation*, 8, pp.1–31.

Fallah-Shojaei, A., Tabatabaeian, K., Shirini, F. and Hejazi, S., 2014. Multi-walled carbon nanotube supported Fe₃O₄ NPs: an efficient and reusable catalyst for one-pot synthesis of 4H-pyran derivatives. *RSC Advances*, [online] 4(19). Available at: <<http://xlink.rsc.org/?DOI=C5TC02043C>>.

Global Market Insights, 2018. *Synthetic & Bio-based Aniline Market Forecast Report 2024*. [online] Available at: <<https://www.openpr.com/news/1347162/Synthetic-Bio-based-Aniline-Market-Forecast-Report-2024-Key-Players-are-BASF-The-Chemours-Company-Huntsman-Corporation-The-Dow-Chemical-Company-Sinopec-Argentina-Exploration-and-Production-Inc-Covestro-Tosoh-Corporation>> [Accessed 26 Jun. 2019].

Huang, Y.-H., Su, C.-C., Yang, Y.-P. and Lu, M.-C., 2012. Degradation of aniline catalyzed by heterogeneous Fenton-like reaction using iron oxide/SiO₂. *Environmental Progress & Sustainable Energy*, 32(2), pp.187–192.

Huang, Z., Xi, L., Subhani, Q., Yan, W., Guo, W. and Zhu, Y., 2013. Covalent functionalization of multi-walled carbon nanotubes with quaternary ammonium groups and its application in ion chromatography. *Carbon*, [online] 62(i), pp.127–134. Available at: <<http://dx.doi.org/10.1016/j.carbon.2013.06.004>>.

Ilic, M., Koglin, E., Pohlmeier, A., Narres, H.D. and Schwuger, M.J., 2000.

Adsorption and polymerization of aniline on Cu(II)-montmorillonite: Vibrational spectroscopy and ab initio calculation. *Langmuir*, 16(23), pp.8946–8951.

Jackson, R.S., 2014. Post-Fermentation Treatments and Related Topics. *Wine Science*, pp.535–676.

Jia, X., Chen, X., Liu, Y., Zhang, B., Zhang, H. and Zhang, Q., 2019. Hydrophilic Fe₃O₄ nanoparticles prepared by ferrocene as high-efficiency heterogeneous Fenton catalyst for the degradation of methyl orange. *Applied Organometallic Chemistry*, 33(4), p.e4826.

Joshi, M., Bhattacharyya, A. and Ali, W.S., 2008. Characterization techniques for nanotechnology applications in textiles. *Indian Journal of Fibre & Textile Research*, 33, pp.304–317.

Jung, Y.S., Lim, W.T., Park, J.Y. and Kim, Y.H., 2009. Effect of pH on Fenton and Fenton-like oxidation. *Environmental Technology*, 30(2), pp.183–190.

Jurková, B., 2013. *Carbon nanomaterials and their interactions with bacteria*. Charles University, Prague.

Kakavandi, B., Jafari, A.J., Kalantary, R.R., Nasser, S., Ameri, A. and Esrafil, A., 2013. Synthesis and properties of Fe₃O₄-activated carbon magnetic nanoparticles for removal of aniline from aqueous solution: Equilibrium, kinetic and thermodynamic studies. *Iranian Journal of Environmental Health Science and Engineering*, 10(19), pp.2–10.

Khan, I. and Saeed, K., 2013. Carbon nanotubes-properties and applications: a review. *Carbon letters*, 14(3), pp.131–144.

Khan, T.A., Nazir, M. and Khan, E.A., 2016. Magnetically modified multiwalled carbon nanotubes for the adsorption of bismarck brown R and Cd(II) from aqueous solution: batch and column studies. *Desalination and Water Treatment*, 57(41), pp.19374–19390.

Kim, J.R., Huling, S.G. and Kan, E., 2015. Effects of temperature on adsorption and oxidative degradation of bisphenol A in an acid-treated iron-amended granular activated carbon. *Chemical Engineering Journal*, 262, pp.1260–1267.

Kong, I., Ahmad, S.H. and Shanks, R., 2016. Properties enhancement in multiwalled carbon nanotube-magnetite hybrid-filled polypropylene natural rubber nanocomposites through functionalization and processing methods. *Science and Engineering of Composite Materials*, 23(3), pp.257–267.

Kukovecz, Á., Kozma, G. and Kónya, Z., 2013. Multi-Walled Carbon

Nanotubes. In: *Springer Handbook of Nanomaterials*. Berlin, Heidelberg: Springer Berlin Heidelberg, pp.147–188.

Li, S., Gong, Y., Yang, Y., He, C., Hu, L., Zhu, L., Sun, L. and Shu, D., 2015. Recyclable CNTs/Fe₃O₄ magnetic nanocomposites as adsorbents to remove bisphenol A from water and their regeneration. *Chemical Engineering Journal*, [online] 260, pp.231–239. Available at: <<http://dx.doi.org/10.1016/j.cej.2014.09.032>>.

Liu, X., Zhang, S. and Pan, B., 2012. Potential of carbon nanotubes in water treatment. *Recent Progress in Carbon Nanotube Research*, pp.1–30.

Liu, Y., Zhang, G., Fang, S., Chong, S. and Zhu, J., 2016. Degradation of aniline by heterogeneous Fenton's reaction using a Ni-Fe oxalate complex catalyst. *Journal of Environmental Management*, 182, pp.367–373.

Mehta, D., Mazumdar, S. and Singh, S.K., 2015. Magnetic adsorbents for the treatment of water/wastewater-A review. *Journal of Water Process Engineering*, 7, pp.244–265.

Minnesota Rural Water Association, n.d. *Coagulation and Flocculation*. [online] Available at: <[https://www.mrwa.com/WaterWorksMnl/Chapter 12 Coagulation.pdf](https://www.mrwa.com/WaterWorksMnl/Chapter%2012%20Coagulation.pdf)> [Accessed 12 Jul. 2019].

Moazzen, M., Mousavi Khaneghah, A., Shariatifar, N., Ahmadloo, M., Eş, I., Baghani, A.N., Yousefinejad, S., Alimohammadi, M., Azari, A., Dobaradaran, S., Rastkari, N., Nazmara, S., Delikhooon, M. and Jahed Khaniki, G.R., 2019. Multi-walled carbon nanotubes modified with iron oxide and silver nanoparticles (MWCNT-Fe₃O₄ /Ag) as a novel adsorbent for determining PAEs in carbonated soft drinks using magnetic SPE-GC/MS method. *Arabian Journal of Chemistry*, [online] 12(4), pp.476–488. Available at: <<https://doi.org/10.1016/j.arabjc.2018.03.003>>.

Moradi, O., 2013. Adsorption Behavior of Basic Red 46 by Single-Walled Carbon Nanotubes Surfaces. *Fullerenes, Nanotubes and Carbon Nanostructures*, 21(4), pp.286–301.

Muruganandham, M., Suri, R.P.S., Jafari, S., Sillanpää, M., Lee, G.-J., Wu, J.J. and Swaminathan, M., 2014. Recent Developments in Homogeneous Advanced Oxidation Processes for Water and Wastewater Treatment. *International Journal of Photoenergy*, 2014, pp.1–21.

Nanot, S., Thompson, N.A., Kim, J.-H., Wang, X., Rice, W.D., Hároz, E.H., Ganesan, Y., Pint, C.L. and Kono, J., 2013. Single-Walled Carbon Nanotubes. In: *Springer Handbook of Nanomaterials*. Berlin, Heidelberg: Springer Berlin Heidelberg, pp.105–146.

Ndi Nsami, J. and Ketcha Mbadcam, J., 2013. The adsorption efficiency of chemically prepared activated carbon from cola nut shells by ZnCl₂ on methylene blue. *Journal of Chemistry*, 2013.

Nie, P., Min, C., Song, H.J., Chen, X., Zhang, Z. and Zhao, K., 2015. Preparation and tribological properties of polyimide/carboxyl-functionalized multi-walled carbon nanotube nanocomposite films under seawater lubrication. *Tribology Letters*, 58(1), pp.1–12.

Nunez, C., 2010. *Water pollution facts and information*. [online] Available at: <<https://www.nationalgeographic.com/environment/freshwater/pollution/>> [Accessed 26 Jun. 2019].

Rafique, I., Kausar, A., Anwar, Z. and Muhammad, B., 2015. Exploration of Epoxy Resins, Hardening Systems, and Epoxy/Carbon Nanotube Composite Designed for High Performance Materials: A Review. *Polymer-Plastics Technology and Engineering*, 55(3), pp.312–333.

Rahmawati, R., Melati, A., Taufiq, A., Sunaryono, Diantoro, M., Yulianto, B., Suyatman, S., Nugraha, N. and Kurniadi, D., 2017. Preparation of MWCNT-Fe₃O₄ Nanocomposites from Iron Sand Using Sonochemical Route. *IOP Conference Series: Materials Science and Engineering*, 202.

Rajisha, K.R., Deepa, B., Pothan, L.A. and Thomas, S., 2011. Thermomechanical and spectroscopic characterization of natural fibre composites. *Interface Engineering of Natural Fibre Composites for Maximum Performance*, pp.241–274.

Ramachandran, P., Sundharam, R., Palaniyappan, J. and Munusamy, A.P., 2013. Potential process implicated in bioremediation of textile effluents: A review. *Pelagia Research Library Advances in Applied Science Research*, 4(1), pp.131–145.

Ratanatamskul, C., Masomboon, N. and Lu, M.-C., 2011. Application of Fenton Processes for Degradation of Aniline. *Pesticides in the Modern World - Pesticides Use and Management*, pp.463–474.

RSC, 2009. *Ultraviolet-Visible Spectroscopy (UV)*. [online] Available at: <<http://www.chemguide.co.uk/analysis/uvvisiblemenu.html#top>> [Accessed 3 Aug. 2019].

Sadegh, H., Shahryari-ghoshekandi, R. and Kazemi, M., 2014. Study in synthesis and characterization of carbon nanotubes decorated by magnetic iron oxide nanoparticles. *International Nano Letters*, 4(4), pp.129–135.

Sarangdevot, K. and Sonigara, B.S., 2015. The wondrous world of carbon nanotubes: Structure, synthesis, properties and applications. *Journal of*

Chemical and Pharmaceutical Research, 7(6), pp.916–933.

SDWF, 2017. *Industrial Waste — Safe Drinking Water Foundation*. [online] Available at: <<https://www.safewater.org/fact-sheets-1/2017/1/23/industrial-waste>> [Accessed 26 Jun. 2019].

Shen, J.-H., Horng, J.-J., Wang, Y.-S. and Zeng, Y.-R., 2017. The use of reactive index of hydroxyl radicals to investigate the degradation of acid orange 7 by Fenton process. *Chemosphere*, 182, pp.364–372.

Sinha, P., Datar, A., Jeong, C., Deng, X., Chung, Y.G. and Lin, L.C., 2019. Surface Area Determination of Porous Materials Using the Brunauer-Emmett-Teller (BET) Method: Limitations and Improvements. *Journal of Physical Chemistry C*, 123(33), pp.20195–20209.

Sivashankar, R., Sathya, A.B., Vasantharaj, K. and Sivasubramanian, V., 2014. Magnetic composite an environmental super adsorbent for dye sequestration – A review. *Environmental Nanotechnology, Monitoring & Management*, 1–2, pp.36–49.

Stoffelbach, F., Aqil, A., Jérôme, C., Jérôme, R. and Detrembleur, C., 2005. An easy and economically viable route for the decoration of carbon nanotubes by magnetite nanoparticles, and their orientation in a magnetic field. *Chemical Communications*, (36), p.4532.

Swapp, S., 2019. *Scanning Electron Microscopy (SEM)*. [online] Available at: <https://serc.carleton.edu/research_education/geochemsheets/techniques/SEM.html> [Accessed 3 Aug. 2019].

Wang, H., Jiang, H., Wang, S., Shi, W., He, J., Liu, H. and Huang, Y., 2014. Fe₃O₄ –MWCNT magnetic nanocomposites as efficient peroxidase mimic catalysts in a Fenton-like reaction for water purification without pH limitation. *RSC Adv.*, 4(86), pp.45809–45815.

Wang, S.H., Wang, T. and Zhou, X., 2017. Recent advances in hybrid measurement methods based on atomic force microscopy and surface sensitive measurement techniques. *RSC Adv.*, 7(75), pp.47464–47499.

Wang, T.O., Huang, J. and Lieber, C.M., 2002. Single-Walled Carbon Nanotubes From Fundamental Studies to New Device Concepts. *Annals New York Academy of Sciences*, 960, pp.203–215.

Wang, W., Mao, Q., He, H. and Zhou, M., 2013. Fe₃O₄ nanoparticles as an efficient heterogeneous Fenton catalyst for phenol removal at relatively wide pH values. *Water Science and Technology*, 68(11), pp.2367–2373.

Worch, E., 2012. *Adsorption Technology in Water Treatment*. Berlin: Walter de Gruyter GmbH & Co. KG.

Zare, K., Kumar Gupta, V., Moradi, O., Salam Hamdy Makhlof, A., Sillanpää, M., Nadagouda, M.N., Sadegh, H., Shahryari-ghoshekandi, R., Pal, A., Wang, Z., Tyagi, I. and Kazemi, M., 2015. A comparative study on the basis of adsorption capacity between CNTs and activated carbon as adsorbents for removal of noxious synthetic dyes: a review. *Journal of Nanostructure in Chemistry*, 5, pp.227–236.

Zhang, M., Dong, H., Zhao, L., Wang, D. and Meng, D., 2019. A review on Fenton process for organic wastewater treatment based on optimization perspective. *Science of The Total Environment*, 670, pp.110–121.

Zhou, L., Zhang, H., Ji, L., Shao, Y. and Li, Y., 2014. Fe₃O₄/MWCNT as a heterogeneous Fenton catalyst: degradation pathways of tetrabromobisphenol A. *RSC Advances*, 4(47), p.24900.

APPENDICES

APPENDIX A: Preparation of Various Concentration of Aniline

The various concentration of aniline can be prepared from a stock solution through dilution with distilled water. The volume of stock solution required to achieve desired concentration of aniline can be calculated as followed:

$$C_1V_1 = C_2V_2$$

where

C_1 = Concentration of stock solution, ppm

V_1 = Volume of stock solution, L

C_2 = Concentration of diluted solution, ppm

V_2 = Volume of diluted solution, L

After the value of V_1 is calculated, the required amount will be pipetted into a small bottle. Distilled water is added to achieved desired volume. To prepare the 500 ppm aniline stock solution in 0.5 L, the calculation is as followed:

Density of aniline = 1.02 g/cm³

Molecular weight = 93.13 g/mol

$$\text{Concentration of stock solution} = 500 \text{ ppm} = \frac{500 \text{ mg}}{1 \text{ L}} = \frac{250 \text{ mg}}{0.5 \text{ L}} = \frac{0.25 \text{ g}}{0.5 \text{ L}}$$

To prepare 500 ppm aniline stock solution, 0.25 of aniline is required to dissolve in 500 ml of distilled water.

Since 1ml of aniline solution =1.02 g of aniline, hence 0.245 ml of aniline is required for 0.25 g of aniline. Hence, aniline stock solution with 500 ppm was prepared by dissolving 0.245 ml of aniline with distilled water in 500 ml volumetric flask.

Volume of 500 ppm stock solution required to prepare various concentration in 15 mL solution is shown in Table A.1. The volume of 500 ppm stock solution required to prepare 15 mL of diluted aniline with 50 ppm concentration is calculated as follow:

$$(500 \text{ ppm})(V_1) = (50 \text{ ppm})(15 \text{ mL})$$
$$V_1 = 1.5 \text{ mL}$$

Hence, 1.5 mL of 500 ppm aniline stock solution is required to dissolved in distilled water to form a 15 mL solution of 50 ppm diluted aniline.

Table A.1: Volume of Aniline Stock Solution Required to Prepare Various Concentration of Aniline in 15 ml solution

Concentration of Aniline (ppm)	Volume of 500 ppm Aniline Stock Solution Required (mL)
10	0.3
20	0.6
30	0.9
40	1.2
50	1.5

APPENDIX B: Preparation of 0.1 M HCl from a 37 % HCl Solution

Molarity of 37 % of HCl is calculated as below:

HCl – 37 % v/v = 37 mL/ 100 mL

Density of 37 % HCl = 1.19 g/mL

Molecular weight of HCl = 36.46 g/mol

$$\begin{aligned}\text{Concentration of HCl } \left(\frac{\text{g}}{\text{L}}\right) &= \frac{37 \text{ mL}}{100 \text{ mL}} \times \frac{1.19 \text{ g}}{\text{mL}} \times \frac{1000 \text{ mL}}{1 \text{ L}} \\ &= 440.3 \frac{\text{g}}{\text{L}}\end{aligned}$$

$$\begin{aligned}\text{Molarity of HCl} &= \frac{440.3 \text{ g}}{\text{L}} \times \frac{1 \text{ mol}}{36.46 \text{ g}} \\ &= 12.07 \text{ mol/L}\end{aligned}$$

The volume of 37 % of HCl required to obtain 0.1 M of HCl is calculated as follow:

$$M_1V_1 = M_2V_2$$

where

M_1 = Concentration of 37 % HCl solution, M

V_1 = Volume of 37 % HCl solution, mL

M_2 = Final concentration of diluted HCl solution, M

V_2 = Volume of diluted HCl solution, mL

$$\begin{aligned}V_1 &= \frac{M_2V_2}{M_1} \\ &= \frac{0.1 \text{ M} \times 500 \text{ mL}}{12.07 \text{ M}} \\ &= 4.14 \text{ mL}\end{aligned}$$

Hence, 4.14 mL of 37 % HCl is required to prepare 500 mL of 0.1 M of HCl solution.

APPENDIX C: Preparation of 0.1 M NaOH from 97 % NaOH

To produce 0.1 M of NaOH in 500 mL solution, the required mass of NaOH pellet is calculated as follow:

$$\begin{aligned}\text{Number of moles of NaOH} &= \text{Molarity} \left(\frac{\text{mol}}{\text{L}} \right) \times \text{Volume(L)} \times \text{purity} \\ &= 0.1 \frac{\text{mol}}{\text{L}} \times 500 \text{ mL} \times \frac{1 \text{ L}}{1000 \text{ mL}} \times \frac{100}{97} \\ &= 0.052 \text{ moles NaOH}\end{aligned}$$

$$\text{MW of NaOH} = 40 \frac{\text{g}}{\text{mol}}$$

$$\begin{aligned}\text{Mass of NaOH} &= \text{Number of moles of NaOH} \times \text{MW of NaOH} \\ &= 0.052 \text{ moles} \times 40 \frac{\text{g}}{\text{moles}} \\ &= 2.08 \text{ g}\end{aligned}$$

Hence, 2.08 g of NaOH is required to be dissolved in 500 mL distilled water to obtain 0.1 M of NaOH solution.

APPENDIX D: Preparation of 0.1 M H₂O₂ from 30 % H₂O₂

In 30 % (w/w) H₂O₂, there is 30 g of H₂O₂ present in 100 g of solution. To convert the concentration to unit of weight per volume (w/V), the calculation is as followed:

$$\rho = \frac{m}{V}$$

where

ρ = Density, g/mL

m = Mass, g

V = Volume, mL

Density of 30 % H₂O₂=1.11 g/ML

$$\begin{aligned} V &= \frac{m}{\rho} \\ &= \frac{100 \text{ g}}{1.11 \frac{\text{g}}{\text{mL}}} \\ &= 90.09 \text{ mL} \end{aligned}$$

$$\begin{aligned} \% \text{ concentration } \left(\frac{w}{V} \right) &= \frac{\text{Amount of solute (g)}}{\text{Amount of solution (mL)}} \times 100\% \\ &= \frac{30 \text{ g}}{90.09 \text{ mL}} \times 100\% \\ &= 33.30 \% \left(\frac{w}{V} \right) \end{aligned}$$

Hence, it indicates that there are 33.30 g of H₂O₂ present in 100 mL solution.

$$\begin{aligned} \text{Moles} &= \frac{\text{Mass of H}_2\text{O}_2}{\text{MW of H}_2\text{O}_2} \\ &= \frac{33.30 \text{ g}}{34.01 \frac{\text{g}}{\text{mol}}} \\ &= 0.98 \text{ mol of H}_2\text{O}_2 \end{aligned}$$

$$\text{Molarity} = \frac{\text{Number of moles of solutes (mol)}}{\text{Volume of solution (L)}}$$

$$\begin{aligned}
 &= \frac{0.98 \text{ mol}}{0.1 \text{ L}} \\
 &= 9.8 \frac{\text{mol}}{\text{L}} \\
 &= 9.8 \text{ M}
 \end{aligned}$$

To produce 0.1 M stock solution of H₂O₂ in 100 mL solution, the calculation is as follow:

$$M_1V_1 = M_2V_2$$

where

M_1 = Concentration of 30 % H₂O₂ solution, M

V_1 = Volume of 30 % H₂O₂ solution, mL

M_2 = Final concentration of diluted H₂O₂ solution, M

V_2 = Volume of diluted H₂O₂ solution, mL

$$(9.8 \text{ M})V_1 = (0.1 \text{ M})(100 \text{ mL})$$

$$V_1 = 1.02 \text{ mL}$$

Hence, 1.02 mL of 30 % H₂O₂ is pipetted and mixed with distilled water to form 100 mL 0.1 M H₂O₂ stock solution. Volume of 0.1 M stock solution required to prepare different concentration of H₂O₂ is calculated using same method and the volume required is tabulated in Table D.1.

Table D.1: Volume of H₂O₂ Required to Prepare Different Dosage in 15 mL Solution

H ₂ O ₂ Dosage (mM)	Volume of 0.1 M H ₂ O ₂ Solution Required (mL)
4.00	0.600
6.43	0.965
10.00	1.500
13.57	2.036
16.00	2.400

APPENDIX E: Calibration Curve of Aniline

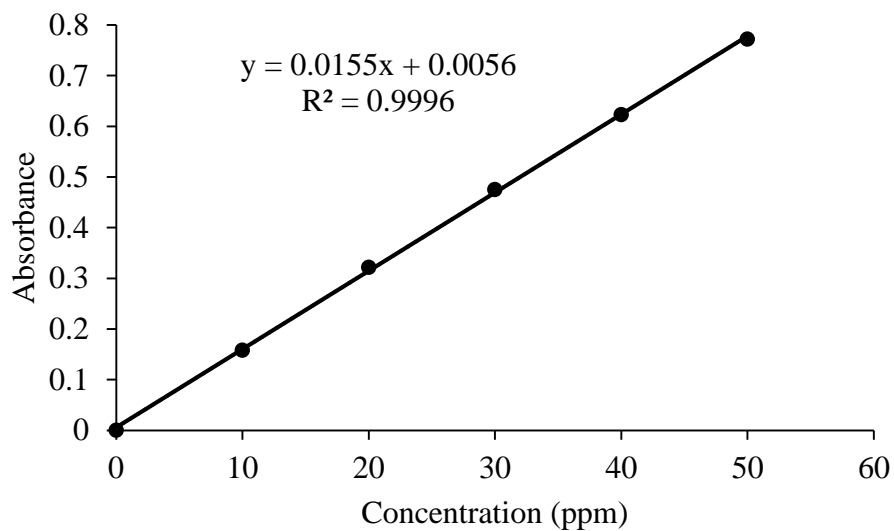


Figure E.1: Calibration Curve of Aniline in Distilled Water

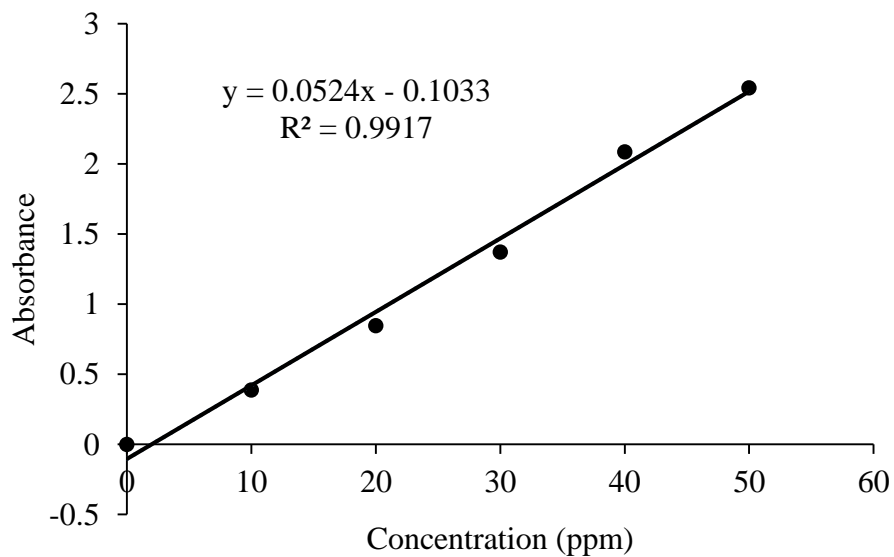


Figure E.2: Calibration Curve of Aniline in Ethanol